Geochimica et Cosmochimica Acta 357 (2023) 77–91

Contents lists available at ScienceDirect

Geochimica et Cosmochimica Acta

journal homepage: www.elsevier.com/locate/gca

Determining the thermal histories of Apollo 15 mare basalts using diffusion modelling in olivine

S.K. Bell [a,b,*], D.J. Morgan [c], K.H. Joy [a], J.F. Pernet-Fisher [a], M.E. Hartley [a]

[a] Department of Earth and Environmental Sciences, University of Manchester, Manchester M13 9PL, UK
[b] Rocktype Ltd, Magdalen Centre, Oxford, UK
[c] School of Earth and Environment, University of Leeds, Leeds LS2 9JT, UK

ARTICLE INFO

Associate editor: Bernard Charlier

Keywords:
Diffusion
Olivine
Mare basalt
Lunar magmatism
Apollo 15

ABSTRACT

Mare basalts collected at the Apollo 15 landing site can be classified into two groups. Based on differing whole-rock major element chemistry, these groups are the quartz-normative basalt suite and the olivine-normative basalt suite. In this study we use modelling of Fe-Mg interdiffusion in zoned olivine crystals to investigate the magmatic environments in which the zonation was formed, be that within the lunar crust or during cooling within a surficial lava flow, helping to understand the thermal histories of the two basalt suites. Interdiffusion of Fe-Mg in olivine was modelled in 29 crystals in total, from six olivine-normative basalt thin sections and from three quartz-normative basalt thin sections. We used a dynamic diffusion model that includes terms for both crystal growth and intracrystalline diffusion during magma cooling. Calculated diffusion timescales range from 5 to 24 days for quartz-normative samples, and 6 to 91 days for olivine-normative samples. Similarities in diffusion timescales point to both suites experiencing similar thermal histories and eruptive processes. The diffusion timescales are short (between 5 and 91 days), and compositional zonation is dominated by crystal growth, which indicates that the diffusion most likely took place during cooling and solidification within lava flows at the lunar surface. We used a simple conductive cooling model to link our calculated diffusion timescales with possible lava flow thicknesses, and from this we estimate that Apollo 15 lava flows are a minimum of 3–6 m thick. This calculation is consistent with flow thickness estimates from photographs of lava flows exposed in the walls of Hadley Rille at the Apollo 15 landing site. Our study demonstrates that diffusion modelling is a valuable method of obtaining information about lunar magmatic environments recorded by individual crystals within mare basalt samples.

1. Introduction

The chemical compositions of crystals in igneous rocks provide a record of the conditions and processes operating within a volcanic system. Olivine is a common mineral in both terrestrial basaltic rocks and lunar basaltic samples (e.g., Papike et al., 1976, 1991). Understanding the magmatic history of lunar basalt samples (known as mare basalts) is important as they provide information about mantle source regions in the lunar interior and the thermal history of the Moon (Neal and Taylor, 1992; Shearer and Papike, 1999; Shearer et al., 2006; Wieczorek et al., 2006 and references therein).

In recent years, Fe-Mg interdiffusion in olivine has been used by many studies to gain a better understanding of terrestrial basaltic magmatic plumbing systems, lava flows, and the timescales over which magmatic processes operate (e.g., Costa and Chakraborty, 2004; Girona and Costa, 2013; Neave et al., 2014; Shea et al., 2015; Rae et al., 2016; Hartley et al., 2016; Viccaro et al., 2016; Kahl et al., 2011, 2013, 2015, 2017; Gordeychik et al., 2018; Pankhurst et al., 2018; Couperthwaite et al., 2020, 2021; Giuffrida et al., 2020). The equilibrium composition of a growing mineral is affected by magmatic variables such as melt composition, temperature, pressure, and oxygen fugacity. A change in magmatic environment may result in the growth of a rim with a different composition to the core, creating a compositional boundary within the crystal, or (in the absence of growth) chemical disequilibrium between the crystal and its surrounding melt. Atoms may then diffuse across crystal core-rim boundary and/or across the crystal-melt interface, as the crystal re-equilibrates with its magmatic environment. Diffusion is a time-dependent process and diffusion coefficients have been established

* Corresponding author at: Department of Earth and Environmental Sciences, University of Manchester, Manchester M13 9PL, UK.
E-mail address: samantha.bell@manchester.ac.uk (S.K. Bell).

https://doi.org/10.1016/j.gca.2023.08.009
Received 13 September 2022; Accepted 7 August 2023
Available online 9 August 2023

for a wide selection of elements and minerals (e.g., Costa and Morgan, 2010). The properties of Fe-Mg interdiffusion in olivine are well-defined for natural samples in terrestrial basaltic systems, and have been experimentally constrained at a variety of compositions, pressures, temperatures, and oxygen fugacities (e.g., Dohmen et al., 2007; Dohmen and Chakraborty, 2007); the oxygen fugacity conditions in these experiments do not replicate the strongly reducing lunar conditions, but have been used previously to model diffusion in lunar samples (e.g. Richter et al., 2021). Diffusion timescales can be quantified by fitting modelled profiles to analysed chemical profiles in compositionally zoned crystals (e.g., Morgan and Blake, 2006; Costa et al., 2008; Costa and Morgan, 2010), providing insights into magmatic processes such timescales of crystal storage.

At the Apollo 15 landing site (26.13222°N latitude, 3.63386°E longitude) two suites of mare basalts are present, distinguishable by differences in whole-rock major element chemistry (ALGIT, 1972); the quartz-normative basalts (bulk rock 47–49 wt% SiO_2, 19–20 wt% FeO and 1–2 wt% TiO_2) and the olivine-normative basalts (bulk rock 44–46 wt% SiO_2, 22–23 wt% FeO and 2–3 wt% TiO_2) (Rhodes and Hubbard, 1973). Average eruption ages for the quartz-normative basalts are 3371 ± 21 Ma (2σ error), and 3287 ± 21 Ma (2σ error) for the olivine-normative basalts (Snape et al., 2019).

Compositionally zoned olivine crystals are commonly found within the Apollo 15 mare basalt collection. Previous modelling of Fe-Mg interdiffusion in olivine from Apollo 15 mare basalts focused on determining the thermal history of sample 15555 (Taylor et al., 1977; Richter et al., 2021). Modelling was initially done using a finite one-dimensional kinetic model by Taylor et al. (1977), who determined a minimum cooling rate of 5°/day for 15555. A recent study by Richter et al. (2021), used magnesium zoning and isotopic fractionation to independently verify that post-crystallisation diffusion occurred in olivine from 15555. However, Fe-Mg interdiffusion in olivine has not been applied to a range of samples within the Apollo 15 mare basalts and comparisons have not been made between samples from the olivine-normative and quartz-normative suites.

The petrogenesis of the olivine-normative and quartz-normative basalts has been disputed (Chappell and Green, 1973; Rhodes and Hubbard, 1973; Lofgren et al., 1975; Ma et al., 1976, 1978; Lindstrom and Haskin, 1978; Ryder and Steele, 1988; Snyder et al., 1997, 1998, 2000; Schnare et al., 2008; Snape et al., 2019; Bell et al., 2023). Some studies propose that the major element variations between the two suites reflects compositional differences within the source regions, or different degrees and depths of partial melting of a compositionally homogeneous source (Rhodes and Hubbard, 1973; Snyder et al., 1997, 1998, 2000; Schnare et al., 2008; Hallis et al., 2014). An alternative hypothesis, based on trace element data, theorises that the two suites could have been produced from melts of the same mantle source region (Schnare et al., 2008). In this scenario, it is proposed that compositional differences arose due the quartz-normative basalts undergoing crystallisation at multiple stages within the lunar crust, compared to the olivine-normative basalts that predominantly crystallised in lava flows on the lunar surface (Schnare et al., 2008). If diffusion timescales for Apollo 15 mare basalts were found to reflect periods of storage within the lunar crust, then this would have implications for the competing petrogenetic models. Alternatively, if diffusion timescales were found to reflect cooling within a lava flow, then this would allow comparisons to be made about the emplacement history of the olivine-normative and quartz-normative basalts. These timescales could also be used to constrain the thickness of individual lava flows by using equations developed to model the cooling of lava flows (Jaeger, 1961). As the Apollo mare basalts were not sampled directly from field outcrops (i.e., all were recovered as rocks from the surficial regolith), this information would be valuable for understanding volcanic flow styles and rates. Methods previously used to estimate the thickness of mare basalt flow units include: degradation models of partially buried impact craters (e.g., Du et al., 2019); crater excavation depth estimates (e.g., Thomson et al., 2009; Weider et al., 2010); radar sounding (Ishiyama et al., 2013) and ground penetrating radar (Lai et al., 2020); gravity measurements (e.g., Gong et al., 2016); crater size-frequency distributions (e.g., Hiesinger et al., 2002); shadow analysis of high-resolution orbital images (e.g., Schaber et al., 1976); flow front height measurements (e.g., Gifford and El-Baz, 1981); and experimentally determined lava flow cooling rates of Apollo samples (e.g., Brett, 1975; Lofgren et al., 1975; Takeda et al., 1975; Grove and Walker, 1977). Some of these methods provide estimates of total mare basalt thickness (e.g., crater excavations depths, radar sounding, and gravity measurements), whilst others provide estimates of individual flow units (e.g., crater size frequency distributions, experimentally determined mare basalt cooling rates). Models of lunar eruption styles, the volume of volatiles released during eruptions, transient lunar atmospheres, and the thermal history of the Moon, would all benefit from better understanding the range of individual mare basalt flow thicknesses (Neal and Taylor, 1992; Shearer and Papike, 1999; Shearer et al., 2006; Wieczorek et al., 2006; Garry et al., 2012; Needham and Kring, 2017). The observation of some lava flow outcrops in the walls of Hadley Rille at the Apollo 15 landing site (ALGIT, 1972; Howard et al., 1972; Swann et al., 1972) also provides a unique opportunity to test the validity of any calculated lava flow thicknesses derived from Fe-Mg interdiffusion in olivine.

Here we present Fe-Mg interdiffusion timescales for compositionally zoned olivine crystals in quartz-normative and olivine-normative Apollo 15 mare basalt thin sections. We compare timescales from the two suites to investigate the magmatic environments in which the zonation was formed, be that within the lunar crust or during cooling within a surficial lava flow. We then consider our results in the context of what the diffusion timescales may tell us about the emplacement history (i.e. lava flow thicknesses) and/or petrogenesis of the Apollo 15 olivine-normative and quartz-normative basalt suites.

2. Sample descriptions

A total of nine Apollo 15 mare basalts were chosen for this study, across both the quartz-normative and olivine-normative suites. Samples were selected based on the presence of olivine and whether the olivine has major element compositional zoning. Images of all of the thin sections used in this study are available in the Supplementary Material. This selection of samples does not represent an exhaustive list of all samples within the Apollo 15 mare basalt collection which have zoned olivine crystals.

Of the nine samples in this study, six of them, 15555, 15016, 15105, 15536, 15545, and 15556, are olivine-normative basalts. Sample 15555 is a coarse-grained mare basalt with ~50% phenocrysts of pyroxene (<3 mm) and ~10–12% rounded olivine phenocrysts (<1.5 mm) in a poikilitic plagioclase matrix (Bell et al., 2020; Richter et al., 2021). The sample is one of the largest (9.614 kg) mare basalt samples collected on the Moon and is thought to represent a relatively primitive magma composition due to its higher MgO content relative to other Apollo 15 mare basalts (Chappell et al., 1972; Mason et al., 1972; Chappell and Green, 1973). Sample 15016, is a vesicular basalt with phenocrysts of olivine and pyroxene in matrix of subophitic pyroxene and plagioclase. The basalt is comprised of ~10% subhedral olivine phenocrysts, the majority of which show some degree of compositional zoning. Although texturally different, the bulk rock chemical composition of 15016 is similar to that of 15555 (e.g. Chappell and Green, 1973). Like 15016, 15556 is also a vesicular basalt with ~5% subhedral phenocrysts of olivine in a subophitic matrix of pyroxene and plagioclase. Sample 15105 is a small 5.6 g rake fragment (Swann et al., 1972; Ma et al., 1976) with a porphyritic texture, containing olivine phenocrysts in a fine-grained matrix of pyroxene, plagioclase and smaller olivine crystals. The olivine phenocrysts comprise ~5% of the sample, are up to 3 mm in size, and are zoned. Sample 15536 was chipped from a boulder at the edge of Hadley Rille and is representative of several basalt samples collected in that area (Mason et al., 1972). The sample shows poikilitic

plagioclase enclosing subhedral to equant crystals of olivine and pyroxene with ~2–3% larger zoned olivine phenocrysts up to 1.5 mm in size. Sample 15545 was also collected from the edge of Hadley Rille (Swann et al., 1972) and shows a similar texture to 15536, with ~3–4% olivine phenocrysts surrounded by smaller olivine and pyroxene in poikilitic plagioclase. Minor phases within the olivine-normative samples included chromite, ilmenite, and silica (e.g. ALGIT, 1972).

Olivine is less commonly found in samples from the quartz-normative suite. As a result only three olivine-bearing quartz-normative samples, 15125, 15485, and 15595, were included in this study. Sample 15125 has a vitrophyric texture and contains ~3% skeletal olivine phenocrysts along with pyroxene phenocrysts in a microcrystalline matrix of needle-like pyroxene and plagioclase (Bell et al., 2020). The chemistry of 15125 is similar to 15597; a sample which is considered to represent a near-primary melt that was quenched from a high temperature (Lofgren et al., 1975; Grove and Bence, 1977; Grove and Walker, 1977). Samples 15485 and 15595 also show the same vitrophyric texture as 15125, with ~1–2% skeletal olivine phenocrysts alongside elongate pyroxene phenocrysts in a similar microcrystalline matrix.

3. Methods

Thin sections were prepared at the NASA Johnson Space Center Apollo curatorial labs, and some have been previously studied by other groups. The olivine-normative thin sections included in this study were 15555,209, 15016,146, 15105,6, 15536,5, 15545,64 and 15556,234. The quartz-normative thin sections selected were 15125,6, 15485,31 and 15595,35. All thin sections were carbon coated prior to analysis.

3.1. Data collection

High-resolution backscattered electron (BSE) maps of each thin section were collected using an FEI QUANTA 650 field emission gun (FEG) scanning electron microscope (SEM) at the University of Manchester. ImageJ version 1.51 (Abràmoff et al., 2004) was used to identify olivine crystals with sigmoidal core-rim greyscale profiles that might be indicative of diffusion processes, since greyscale is directly correlated with olivine forsterite content (Costa and Morgan, 2010). Not all olivine crystals in the samples display such profiles; this is due to the effects of the sectioning angle, other crystals impeding growth and diffusion, and the 3D texture of the sample (e.g., Shea et al., 2015; Couperthwaite et al., 2021).

The major element compositions of these olivine crystals were analysed using a Cameca SX100 electron microprobe (EPMA) at the University of Bristol. Analyses were performed using an accelerating voltage of 20 keV, a 20 nA beam current and a 1 μm spot size. Standards used were; albite for Na and Si, olivine for Mg, sanidine for Al and K, wollastonite for Ca, ilmenite for Fe and Ti, and pure metals for Cr, Mn and Ni. Line traverses were taken perpendicular to the crystal edge from the rim to the core, with measurements made at either ~5, 10 or 20 μm intervals, giving 10–20 points per profile. All the traverse paths and EPMA data are reported in full in the Supplementary Material.

Diffusion of Fe and Mg in olivine is strongly anisotropic and diffusion rates vary by a factor of six depending on crystallographic orientation (Dohmen and Chakraborty, 2007). The crystallographic orientations of the olivine crystals were determined using electron backscatter diffraction (EBSD). Measurements were made using a TESCAN MIRA3 SEM with an Oxford Instruments Symmetry EBSD detector at the University of Manchester. Crystallographic orientations were gathered using Oxford Instruments software Aztec 4.2. Euler pole angles were used to calculate the plunge and trend of [1 0 0], [0 1 0] and [0 0 1] relative to the thin section plane. Corrections for the diffusion coefficient in the direction of the traverse were made by calculating the angle between the crystallographic axes of the crystal and the measured EPMA traverse (Costa and Chakraborty, 2004).

3.2. Diffusion modelling

Diffusion modelling studies, including those of Fe-Mg interdiffusion in olivine, have commonly employed isothermal diffusion models, where the temperature of the system is assumed to be constant and at equilibrium (e.g., Allan et al., 2013; Girona and Costa, 2013; Hartley et al., 2016; Pankhurst et al., 2018; Couperthwaite et al., 2020). Isothermal diffusion models are appropriate for olivine found in terrestrial volcanic tephra samples, where crystals stored at near-constant temperature in a magma reservoir are near-instantaneously quenched upon eruption (Hartley et al., 2016; Pankhurst et al., 2018). However, in magmatic environments where temperature is variable through the different stages of magma storage, transport and eruption, non-isothermal diffusion models are required (e.g., Costa et al., 2008). In this study we have used the Fe-Mg interdiffusion model developed for terrestrial basaltic samples by Couperthwaite et al. (2021) as it is an advanced dynamic model that takes into consideration the effects of crystal growth and changes in boundary conditions as crystallisation proceeds through a changing temperature regime, such as a cooling lava flow. To achieve this, diffusion is modelled as a function of temperature, since diffusion, growth and equilibrium olivine composition are all driven by the temperature of the magmatic environment (Couperthwaite et al., 2021). The diffusion model is an iterative one-dimensional finite difference model that simultaneously accounts for crystal growth, magma cooling, and Fe-Mg interdiffusion. The model is described in detail in Couperthwaite et al. (2021) and a summary of the calculation steps involved is shown in Fig. 1.

Input variables required by the model are: the olivine core composition (as Fo = 100 × Mg/[Mg + Fe + Mn]), the starting temperature at which the olivine core composition crystallised, oxygen fugacity, pressure, crystallographic orientation, cooling rate, and growth rate. In all models, to match the conditions of lunar mare basalt lava flows, pressure was set as 1 bar and oxygen fugacity was set to $\log(fO_2) = \Delta IW-1$ (Wadhwa, 2008). The olivine core composition was determined by EPMA and crystal orientation by EBSD analysis. Growth rates and cooling rates were varied to find a combination that produced a model which best fitted the measured olivine zoning profiles. For the model to be accurate, and to determine the temperature-composition relationship during cooling, the equilibrium composition of olivine needs to be parameterised as a function of temperature (Couperthwaite et al., 2021). Temperature parametrisation was achieved for each sample using temperature and olivine Fo composition data calculated in MELTS (Gualda et al., 2012; Ghiorso and Gualda, 2015). For each sample we used bulk rock compositions from the literature as starting compositions for the MELTS calculations (Table 1), and we assume fractional crystallisation. The pressure, oxygen fugacity, suppression of certain crystallising phases, and temperature range used in MELTS calculations, were specified to best reflect lunar conditions (see Supplementary Material for details). We are aware that MELTS does not necessarily utilise lunar-specific mineral distribution coefficients (Slater et al., 2003; Thompson et al., 2003). Despite this, MELTS calculations are still applicable at lunar conditions and have been used in many other studies of mare basalts (e.g., Anand et al., 2003, 2006; Joy et al., 2006; Li et al., 2016; Richter et al., 2021).

A Monte Carlo simulation was used to estimate the effect on diffusivity associated with a temperature uncertainty of ±30 °C and an oxygen fugacity uncertainty of ±0.5 log units. The relatively minor errors associated with measured profile length (±2%), EPMA measurements (~0.1 mol.% on Fo), and the uncertainty on the diffusivity value for Fe-Mg in olivine, were also accounted for in the simulation. A maximum uncertainty of 0.41 log units (1σ) was determined for the diffusion timescales in this study (see supplementary Fig. S1 for further details). As the uncertainty is not normally distributed in linear space, a calculated diffusion timescale of 20 days, for instance, would equate to a timescale uncertainty range of 7.8–51 days.

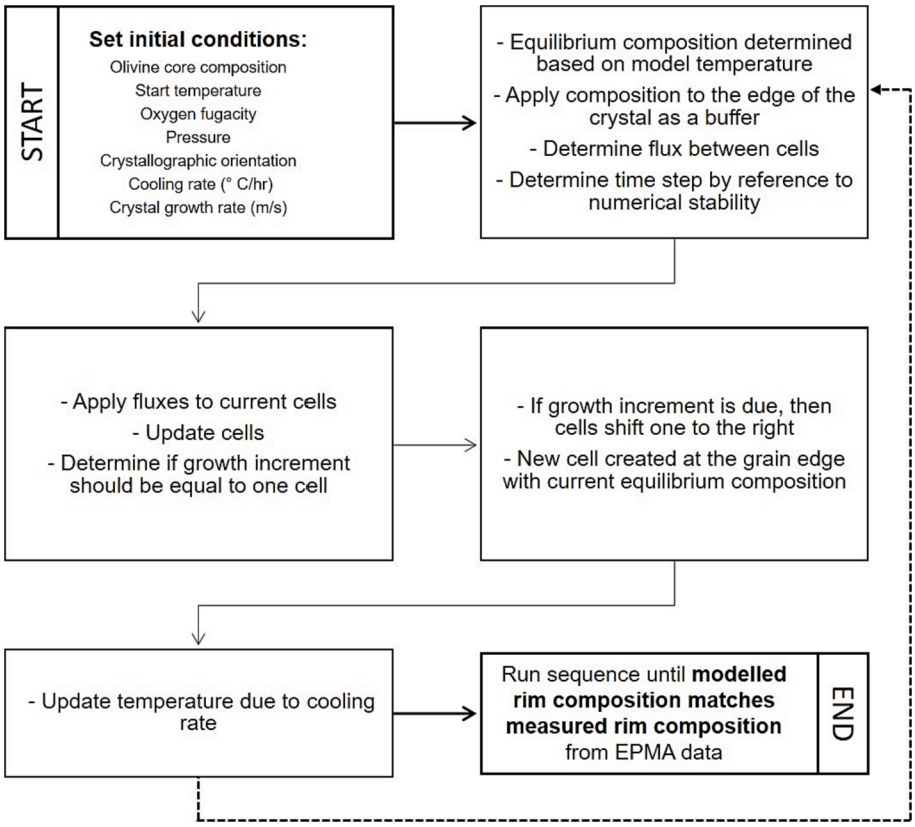

Fig. 1. Schematic diagram showing the workflow of the dynamic diffusion model (after Couperthwaite et al., 2021).

4. Results

4.1. Mineral composition

We obtained EPMA analyses for a total of 48 compositionally zoned olivine crystals: 37 in olivine-normative thin sections and 11 in quartz-normative thin sections. The locations of the EPMA profiles are shown in Supplementary Figs. S3–S11. All olivine crystals showed simple normal zoning from a higher-Mg core to a low-Mg rim. Collectively, the highest olivine Fo content in the cores of individual crystals ranged from Fo_{71} to Fo_{49}, and the lowest olivine Fo content rim compositions (i.e., the EPMA point closest to the crystal edge) ranged from Fo_{48} to Fo_{15} (Fig. 2). The maximum and minimum values for core and rim compositions were all observed in olivine crystals from olivine-normative basalt thin sections (Table 1). The range in compositions for the quartz-normative samples was more restricted: Fo_{71} to Fo_{62} for the cores, and Fo_{45} to Fo_{27} for the rims (Table 1).

4.2. Temperature parameterisation

Plots of melt temperature against equilibrium crystallised olivine composition (Fo) were created from the MELTS calculations for each sample (Fig. 2). The trends produced were parameterised using a series of linear fits and incorporated into the diffusion models to calculate equilibrium Fo as a function of temperature. Graphs showing the temperature parameterisation fits for each sample can be found in supplementary Fig. S2.

For olivine-normative samples 15555, 15536, 15545 and 15016, MELTS calculations do not output a continuous range of olivine compositions covering the temperature from the liquidus to ~1030 °C (Fig. 2). There are two separate temperature intervals over which olivine is predicted to crystallise: one at temperatures around 1255–1190 °C crystallizing olivine compositions ranging from Fo_{78} to Fo_{65}, and a second at temperatures around 1095–1040 °C crystallizing olivine compositions of Fo_{37} to Fo_4 (Fig. 2). Such 'gaps' in olivine compositions are also seen in terrestrial systems such as the Skaergaard intrusion (e.g., Wager, 1960), with pyroxene (augite) crystallisation dominating over the compositional gap and the return of fayalitic olivine to the liquidus possibly attributed to the relative instability of Fe-rich pyroxene (i.e., ferrosilite species), such that quartz + fayalite is more stable. The Apollo 15 olivine-normative basalts contain olivine with compositions that plot within the compositional gaps of our MELTS calculations, suggesting that MELTS is not able to capture the full complexity of Apollo 15 liquid lines of descent (see Section 5.1). Therefore, to parameterise the changing olivine composition over the full temperature range, we used a straight-line segment to connect the two crystallisation trends (see the dashed lines in Fig. 2). The implications of this assumption and the arising impacts are discussed in Section 5.1.

For all three quartz-normative samples (15125, 15485 and 15595) and two of the olivine-normative samples (15105 and 15556), the only olivine compositions predicted in MELTS were Fo_{28} to Fo_5, over a temperature interval of 1080–1030 °C (Fig. 2). However, measured olivine crystals in these five samples had core compositions of at least Fo_{60}. To parameterize the high-temperature crystallisation of more forsteritic olivine cores in these samples, we used the high-temperature part of the MELTS crystallisation trend for olivine-normative sample 15536. We also tested our diffusion models using high-temperature portions of the MELTS simulations for other olivine-normative samples (15016 and 15555), but these combinations of temperature parameterizations were not satisfactory as they caused disjunctions in the modelled profiles.

4.3. Fe-Mg Interdiffusion timescales

Of the 48 olivine crystals analysed using EPMA, modelled diffusion profiles were successfully fitted to 29 crystals: 22 from olivine-

Table 1
Apollo sample literature bulk rock compositions used in MELTS simulations to parameterise equilibrium olivine composition as a function of temperature. Full details of the MELTS input parameters can be found in supplementary Table S1. ON = olivine-normative, QN = quartz-normative.

Sample	Group	SiO_2 (wt%)	TiO_2 (wt%)	Al_2O_3 (wt%)	FeO (wt%)	MnO (wt%)	MgO (wt%)	CaO (wt%)	Na_2O (wt%)	K_2O (wt %)	P_2O_5 (wt%)	Cr_2O_3 (wt%)	Total	Mg#	MELTS Liquidus Temp (°C)	MELTS first mineral on liquidus	MELTS Temp olivine first on liquidus (°C)	MELTS Temp olivine last on liquidus (°C)	MELTS olivine Fo range
15016*	ON	44.26	2.29	8.52	22.93	0.31	10.84	9.43	0.32	0.05	0.08	0.80	99.83	0.32	1372	Spinel	1252	1052	73–13
15105§	ON	45.90	2.97	8.20	22.70	0.24	9.00	10.20	0.32	0.03	0.09	0.35	100.00	0.28	1213	Cpx	1083	1028	28–5
15536‡	ON	44.40	2.30	7.66	23.24	0.31	11.11	9.53	0.25	0.04	0.04	0.60	99.48	0.32	1288	Spinel	1258	1028	74–5
15545*	ON	44.89	2.49	8.71	22.43	0.31	10.08	9.95	0.45	0.04	0.07	0.54	99.96	0.31	1285	Spinel	1235	1025	72–4
15555§	ON	44.56	1.10	10.44	19.52	0.25	12.28	10.40	0.30	0.02	0.04	n.r.	98.91	0.39	1286	Olivine	1281	1051	78–10
15556**	ON	46.18	2.64	9.85	21.70	0.32	8.03	10.72	0.30	0.09	0.07	0.77	100.67	0.27	1377	Spinel	1083	1028	27–5
15125†	QN	47.50	2.27	8.30	22.30	0.27	9.40	9.30	0.33	0.05	0.08	0.54	100.34	0.30	1274	Spinel	1079	1029	25–6
15485††	QN	47.39	1.77	9.14	19.82	0.27	9.48	10.21	0.28	0.03	0.08	0.58	99.05	0.32	1329	Spinel	1074	1029	22–6
15595*	QN	48.07	1.77	9.06	20.23	0.30	9.21	10.52	0.35	0.05	0.07	0.52	100.15	0.31	1304	Spinel	1079	1029	24–5

Literature references for bulk rock compositions:
* Chappell and Green (1973).
† Dowty et al. (1973).
‡ Shervais et al. (1990).
§ Hallis et al. (2014).
** Mason et al. (1972).
†† Duncan et al. (1976).

normative basalts and 7 from quartz-normative basalts (Fig. 3). The length of the measured diffusion profiles from rim to core ranged from 40 to 486 μm in olivine-normative samples and from 23 to 91 μm in quartz-normative samples. We slightly adjusted the algorithm used by Couperthwaite et al. (2021). In the original work, the diffusivity determines the size of the time step, and the model was applied to samples that were quenched from high temperature where diffusion was fast and time steps small. In our Apollo 15 samples, diffusion continues down to quite cool temperatures where multiple growth increments could occur within a single diffusion time increment. This led to numerical problems, so we adjusted the model to select whichever timestep is smaller: the diffusion timestep or the time for a growth increment at the scale of interest. For each crystal, the start temperature of the diffusion model was set by using the measured olivine core composition to ascertain the corresponding crystallisation temperature from the MELTS Fo vs. temperature parameterisation (Fig. 2). Starting temperatures were 1190–1238 °C (average 1215 °C) for olivine in quartz-normative samples, and 1133–1238 °C (average 1177 °C) for olivine in olivine-normative samples (see Table 2 for details). We also assumed a linear growth rate for all the olivine crystals.

Initial iterations of the model, where both cooling rate and growth rate were varied to provide a best fit, showed that the best fits to our olivine composition profiles were obtained using crystal growth rates of 2×10^{-12}–6×10^{-11} m/s and cooling rates of 0.035–1 °C/hr (see Supplementary Material). The cooling rate required to fit the model to the olivine zonation profiles is proportional to the growth rate, and so multiple solutions to the same measured profiles can be found by proportionally increasing or decreasing these variables (Fig. 4). Eventually, increasing the cooling rate and growth rate would result in a point being reached where so little diffusion is taking place that growth is then completely dominant. As such, acceptable model fits sit somewhere in between a pure isothermal diffusion curve and a pure growth curve.

In the initial model iterations, when both cooling rate and growth rate where being varied to determine a best fit, we identified a common growth rate of 2×10^{-11} m/s for many of the crystals. Fig. 5, shows a graph of the growth rates used in these initial model iterations. In 25% of the initial model iterations a growth rate of 2×10^{-11} m/s used, and >50% of initial iterations provided a model fit when using growth rates of between 1.5×10^{-11} m/s and 2.5×10^{-11} m/s. We observe a trade-off between the crystal growth rate and the calculated diffusion timescale. Therefore, in order to systematically compare calculated diffusion timescales between crystals, both within the same sample and between samples, we then re-ran the models and calculated diffusion timescales with a fixed growth rate of 2×10^{-11} m/s. Using this fixed crystal growth rate means that varying the cooling rate effectively tunes the ratio of diffusion to growth to produce the required amount of curvature in the model profiles to fit the measured profiles. A model with a growth rate of 0 m/s would be a diffusion-only profile that includes temperature and boundary condition changes with time, and can therefore be regarded as a more complex progression of the simple isothermal model. If we selected a faster growth rate, for example 4×10^{-11} m/s, then the cooling rates required to fit the models proportionally increase, and the calculated diffusion timescales proportionally decrease. However, initial runs that also provided a model fit using faster growth rates still result in diffusion timescales on the order of days which is the same order of magnitude as the models run at a growth rate of 2×10^{-11} m/s (Fig. 5).

The olivine crystal growth rate estimate of 2×10^{-11} m/s is comparable to experimentally determined olivine growth rates in crystallising terrestrial basalts that are also used to study lunar basalts (see Section 5.2). When a constant growth rate of 2×10^{-11} m/s is used, cooling rates required to fit the model to the measured diffusion profiles range from 0.035 to 0.8 °C/hr (Table 2). The average cooling rate was 0.16 °C/hr for the olivine-normative samples and 0.5 °C/hr for the quartz-normative samples.

With a fixed growth rate of 2×10^{-11} m/s, we calculated Fe-Mg interdiffusion timescales for olivine-normative samples of between 6

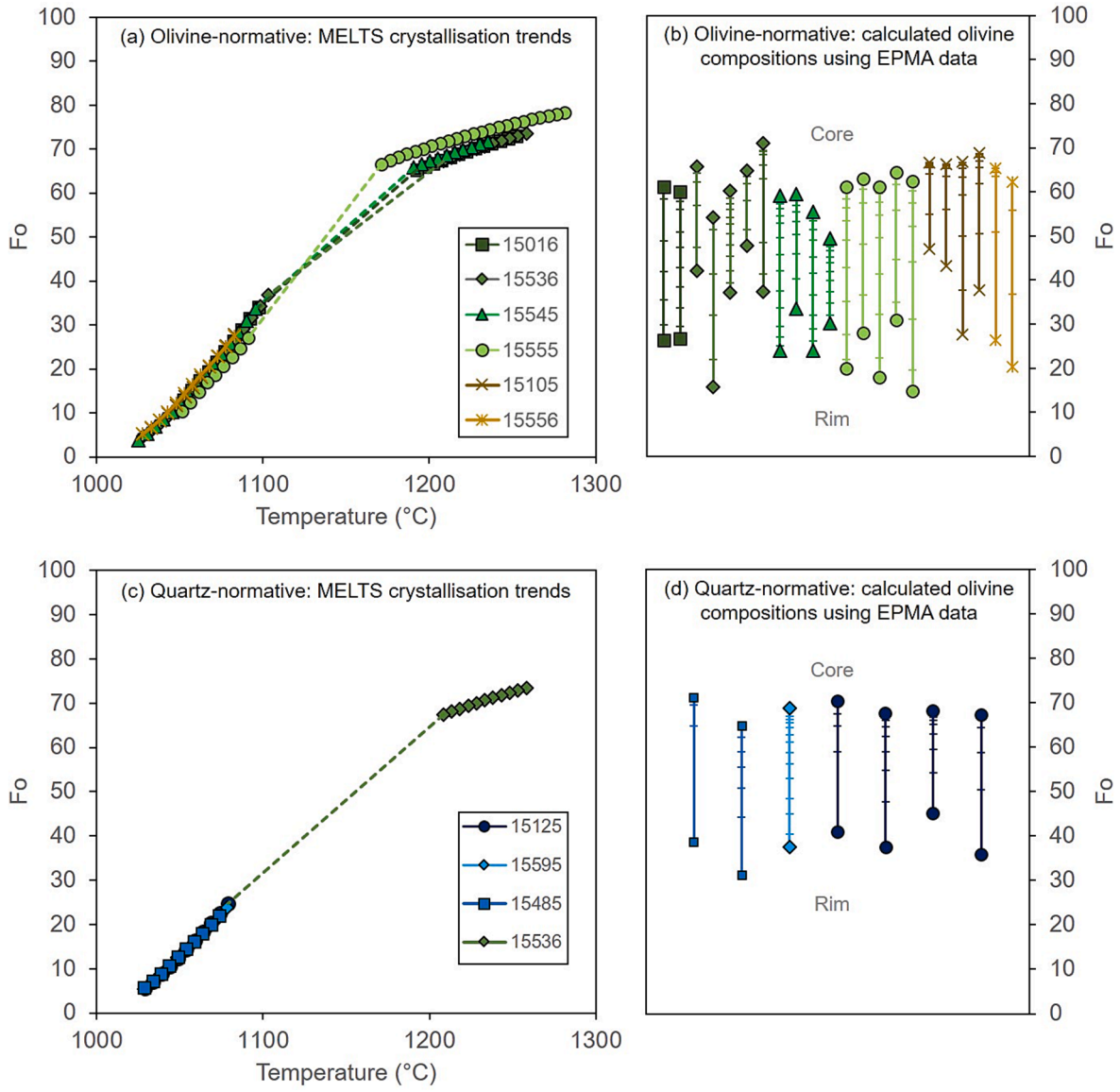

Fig. 2. Plots of temperature vs. Fo using MELTS fractional crystallisation trends, for olivine in olivine-normative samples (a) and quartz-normative samples (c). The plots also show the temperature at which olivine first appears on the liquidus and its composition. The MELTS fractional crystallisation trend for olivine-normative sample 15536 was used to parameterise high-temperature crystallisation for all quartz-normative samples and for olivine-normative samples 15105 and 15556. Calculated olivine compositions using EPMA data are also shown for individual crystals within the olivine-normative (b) and quartz-normative (d) samples.

and 91 days (Fig. 6). Only one olivine crystal returns a timescale of >68 days, with the average timescale of olivine-normative samples being 38 days. For olivine crystals from quartz-normative samples, timescales were 5–24 days (Fig. 6). The average timescale for quartz-normative samples was 10 days, with only two out of the seven crystals showing timescales of >10 days. The average timescale including all crystals from both Apollo 15 mare suites was 31 days.

5. Discussion

A simple isothermal diffusion model (e.g., Hartley et al., 2016; Pankhurst et al., 2018; Couperthwaite et al., 2020) is not suitable for modelling Fe-Mg interdiffusion in olivine from the Apollo 15 mare basalt samples. This is because the measured Fe-Mg profiles in this study show more curvature at the core and an inflection at the rim of the crystal, which are not present in diffusion models calculated assuming isothermal conditions (Fig. 3). This results in a poor-quality fit between measured compositional profiles and an isothermal diffusion model (see Fig. 3 and Fig. S12). The majority (~70%) of diffusion profiles in this study cannot be modelled by simple isothermal diffusion. A similar observation was obtained for olivine from Piton de la Fournaise, La Réunion by Couperthwaite et al. (2021), which led to their use of a dynamic diffusion model that considers simultaneous cooling, crystal growth and diffusion. By using a dynamic diffusion model, we can gather information about the Apollo 15 magmatic system using olivine diffusion profiles that might otherwise have been rejected as unsuitable for diffusion modelling.

5.1. When is olivine on the liquidus?

The MELTS fractional crystallisation calculations predicted a gap in the olivine crystallisation, whereby olivine leaves the liquidus at approximately 1180 °C (Fo_{65}) and re-joins the crystallizing assemblage at approximately 1110 °C (Fo_{30}) (Fig. 2a and c; note that the predicted temperatures and olivine compositions for the crystallisation gap vary by sample). However, our Apollo 15 samples contain olivine crystals

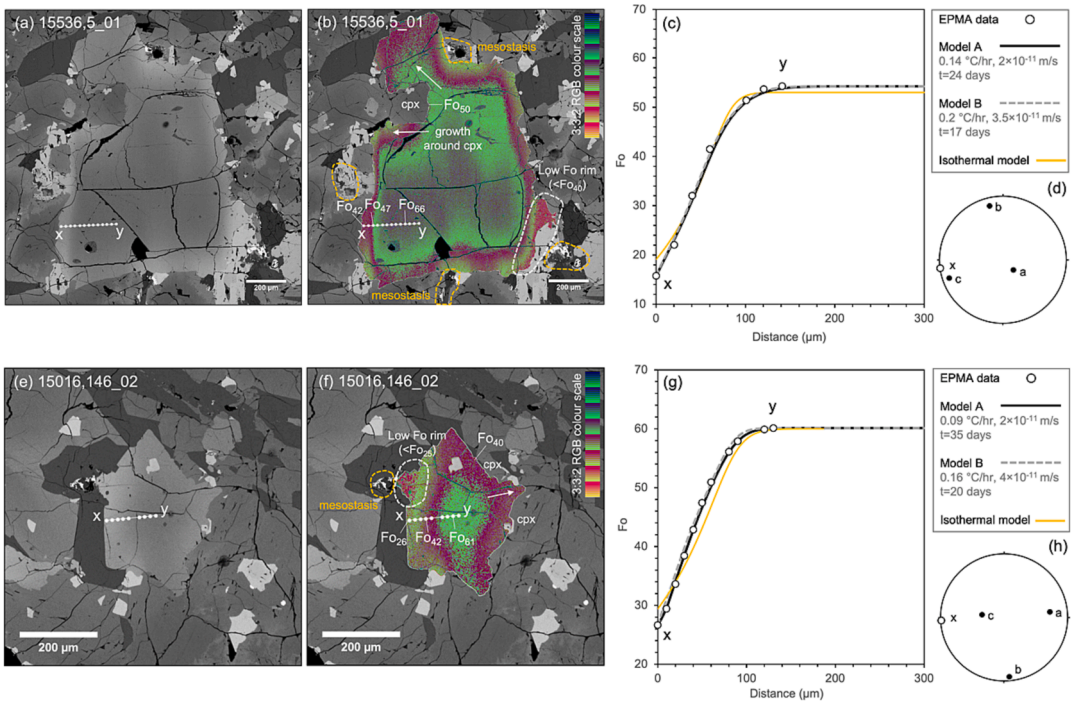

Fig. 3. Examples of backscattered electron images of olivine crystals in (a) 15536,5 and (e) 15016,146. In (b) and (f), the BSE image has been overlain with a 3–3-2 RGB colour scheme to highlight gradients in the compositional zoning. Locations of measured EPMA profiles are shown as a string of white circles, with a selection of Fo values labelled. In both examples the olivine crystals show zoning from >Fo_{60} in the core (lime green) to low-Fo rims (purple to yellow to red). The dashed white lines indicate the lowest Fo values for each crystal. White arrows indicate olivine growth around adjacent clinopyroxene crystals (cpx). Dashed yellow lines indicate areas of mesostasis surrounding the olivine crystals, often associated with the low-Fo rims. Corresponding plots (c) and (g) of olivine composition against distance from the crystal boundary (x to y labelled in all panels) show measured EPMA data points in white circles. Solid black lines show modelled profiles calculated using a growth rate of 2×10^{-11} m/s and cooling rates of 0.14 °C/hr for (c) 15536,5_01 and 0.09 °C/hr for (g) 15016,146_02. Dashed grey lines show alternative modelled profiles calculated using a combination of faster growth rates and cooling rates. Upper hemisphere projections (d) and (h) show crystallographic axes a, b and c, and the orientation of the EPMA traverse (x).

with core compositions that fall within the 'gap' predicted in the MELTS calculations. Our measured profiles show no evidence of disjunctions in minor elements such as Mn or Ni that might suggest that these intermediate-Fo cores might be the result of complete diffusional re-equilibration between a high-Fo core and a lower-Fo rim, or a more evolved carrier melt with an absence of growth over intermediate temperatures, as might be suggested by the MELTS calculations. We have, therefore, opted to use an olivine temperature parameterization that includes continuous growth, using a linear trend to parameterize the no-crystallisation interval predicted by MELTS (dashed lines in Fig. 2a, c).

Diffusion studies of olivine in terrestrial lava flows have noted similar discrepancies between observed olivine compositions and those predicted by crystallisation models such as MELTS or Petrolog3. For example, olivine from Piton de la Fournaise show a smooth transition from Fo_{84} to Fo_{65}, whereas Petrolog3 crystallisation models for this melt predict no olivine more evolved than Fo_{79}, and that olivine is then replaced by orthopyroxene on the liquidus (Couperthwaite et al., 2021). However, the samples themselves contain no orthopyroxene. Thus, despite the Petrolog3 model outputs, there must have been an olivine liquidus in existence between Fo_{79} and Fo_{65}, during which the olivine had time to interact with ambient melt.

If high-Fo olivine is in contact with a more evolved melt, then the olivine must either dissolve; re-equilibrate to approach local chemical equilibrium; or be mantled by growth of the new liquidus phase, i.e. orthopyroxene. As with Piton de la Fournaise (Couperthwaite et al., 2021), we do not observe any olivine being mantled by orthopyroxene (or any other phase) in any of our Apollo 15 samples; nor do we find evidence of crystal dissolution (Fig. 3). This indicates that, in a no-growth scenario, cation exchange between olivine and melt was still taking place across the crystal-melt interface. This raises the possibility of continued olivine growth, despite the theoretical liquidus calculated by MELTS. Retention of olivine-melt equilibrium is critically dependent on the degree of undercooling between the theoretical liquidus and what actually happened in the system during cooling. Mild undercooling could cause a broadening of the olivine-orthopyroxene peritectic region into a diffuse band where olivine could remain stable on the liquidus and continue to grow.

We performed an additional test diffusion model (Supplementary Material Data 2) to illustrate a melt evolution scenario that exactly follows the olivine crystallisation path predicted by MELTS. In this test, we do not permit olivine to grow once it leaves the liquidus. Only diffusion is permitted until the temperature at which Fo returns to the predicted MELTS liquidus. The model then proceeds with both growth and diffusion. After several iterations, we were able to establish a model fit to the measured profile (Supplementary Material Data 2) with a calculated diffusion timescale approximately twice as long (87 days for 15536,5_03) as when continuous olivine growth is permitted (46 days for 15536,5_03 with a growth rate of 2×10^{-11} m/s). Note though that the calculated timescales still remain on the order of days.

That we observe a continuous range in olivine core compositions from Fo_{71} to Fo_{49} in the Apollo 15 samples with no evidence for dissolution or mantling of high-Fo cores (Supplementary Figs. S3–S11) suggests that our MELTS calculations have not fully captured the complexity of crystallisation in this lunar basaltic system. The simplest explanation of our observations is that olivine continued to grow throughout the crystallisation history of the Apollo 15 mare basalts; this interpretation is similar to that of Couperthwaite et al. (2021) to explain the $Fo_{<79}$ olivines in terrestrial Piton de la Fournaise basalts. We acknowledge the possibility that this is not the only solution that can be modelled.

Table 2
Diffusion modelling input parameters and calculated Fe-Mg interdiffusion timescales for each of the olivine crystals in this study using a fixed growth rate of 2×10^{-11} m/s. Different crystals within the same thin section are numbered_01,_02 etc. Timescale uncertainty ranges were calculated using a maximum uncertainty of 0.41 log units (1σ) (see Section 3.2 and supplementary Fig. S1 for further details). Crystal orientation data and model runs using other growth rates can be found in the Supplementary Materials.

Olivine Crystal	Group	Olivine Core (Fo)	Olivine Rim (Fo)	MELTS temp (°C) at core Fo value	Cooling rate (°C/hr)	Calculated Diffusion Timescale (days)	Timescale uncertainty range (days)
15016,146_01	ON	61.0	26.4	1162	0.058	58	23–150
15016,146_02	ON	60.1	26.6	1157	0.09	35	14–91
15105,6_01	ON	66.7	47.0	1190	0.38	7	3–17
15105,6_02	ON	66.2	43.1	1189	0.45	7	3–17
15105,6_03	ON	66.8	27.6	1190	0.23	21	8–54
15105,6_04	ON	68.8	37.7	1217	0.3	17	6–43
15536,5_01	ON	65.7	42.1	1205	0.14	24	9–61
15536,5_02	ON	54.2	15.7	1167	0.09	46	18–118
15536,5_03	ON	60.2	37.1	1187	0.07	48	19–123
15536,5_04	ON	64.7	47.7	1202	0.08	30	12–78
15536,5_05	ON	71.0	37.3	1238	0.09	60	23–155
15545,64_01	ON	59.2	23.9	1162	0.06	61	24–156
15545,64_02	ON	59.5	33.4	1162	0.06	46	18–119
15545,64_03	ON	55.4	24.0	1150	0.07	45	17–115
15545,64_04	ON	49.4	30.2	1133	0.035	52	20–134
15555,209_01	ON	61.2	20.0	1162	0.04	91	35–233
15555,209_02	ON	63.0	27.9	1164	0.1	29	11–76
15555,209_03	ON	61.1	18.0	1162	0.07	55	21–141
15555,209_04	ON	64.5	31.0	1167	0.075	38	15–97
15555,209_05	ON	62.4	14.7	1163	0.095	44	17–114
15556,234_01	ON	65.4	26.3	1192	0.3	16	6–41
15556,234_02	ON	59.3	20.3	1162	0.7	6	2–15
15125,6_01	QN	67.3	35.8	1208	0.8	5	2–13
15125,6_02	QN	68.1	45.0	1213	0.6	5	2–13
15125,6_03	QN	67.6	37.6	1208	0.5	7	3–19
15125,6_04	QN	70.3	40.9	1228	0.5	8	3–21
15485,31_01	QN	64.8	31.1	1190	0.35	11	4–29
15485,31_02	QN	71.1	38.6	1238	0.6	8	3–21
15595,35_01	QN	68.8	37.6	1218	0.2	24	9–62

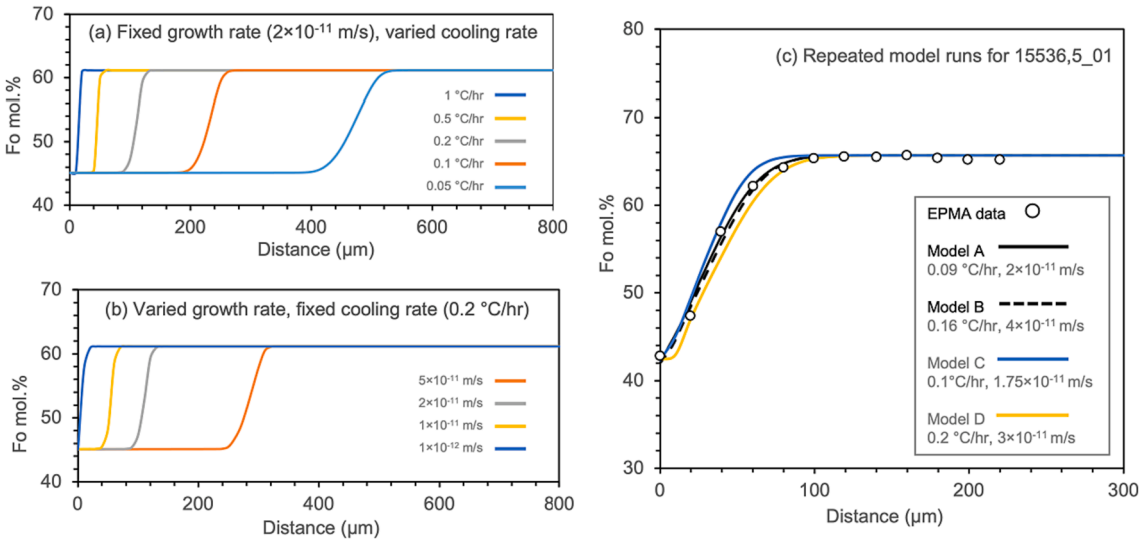

Fig. 4. A sequence of diffusion model runs to show how the diffusion profiles are affected by (a) changes in cooling rate (whilst maintaining a fixed growth rate of 2×10^{-11} m/s) and (b) changes in growth rate (whilst maintaining a fixed cooling rate of 0.2 °C/hr). The combination of growth rates and cooling rates were varied for each run to obtain the best-fit model profile to the measured EPMA data. (c) An example of repeated model runs and their growth and cooling rate values for an olivine crystal in 15536,5. Model runs A (solid black line) and B (dashed grey line) are those that were visually identified as being good fits to the measured diffusion profile.

5.2. *Diffusion model variables – Olivine growth rate*

Olivine growth rates have been used in other studies of olivine in Apollo mare basalt samples to determine crystal residence times in crystal size distribution analysis (Donohue and Neal, 2015; Neal et al., 2015; Bell et al., 2020), and are taken from experimental studies which use various methods to determine olivine growth rates in terrestrial basalts. We are not aware of olivine growth rates determined specifically for lunar compositions under lunar P-T-f_{O2} conditions. Examples of terrestrial olivine growth rates used in crystal size distribution analysis

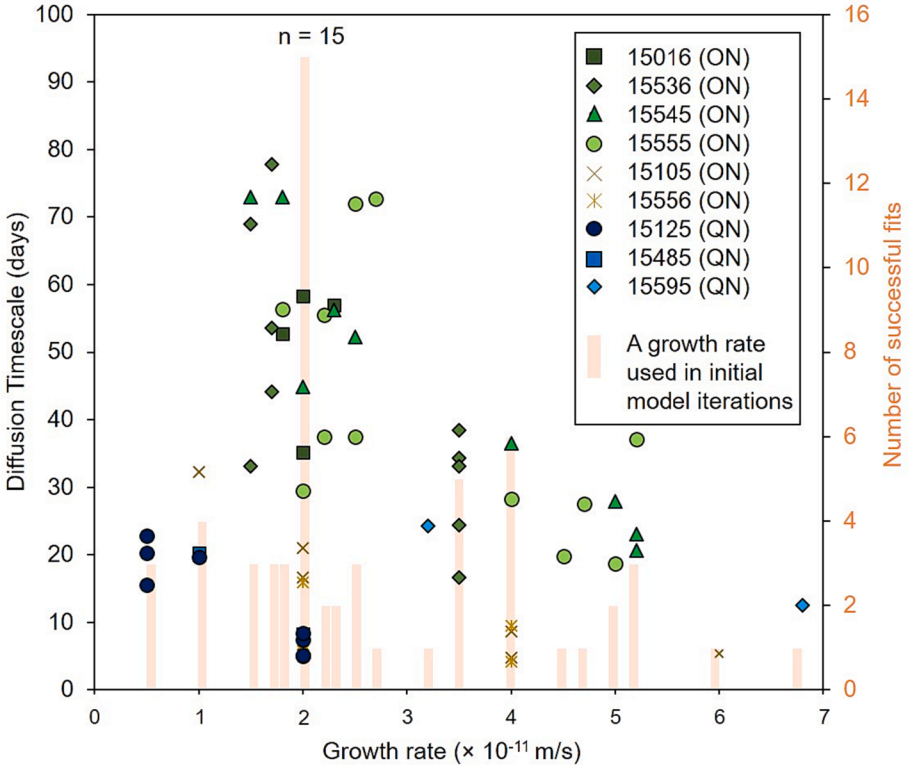

Fig. 5. Diffusion timescales vs the growth rate used in the initial model runs for individual crystals from each of the quartz-normative (QN) and olivine-normative (ON) samples. In the initial model runs both growth rate and cooling rate were varied to determine a best-fit model for each crystal. The secondary y-axis (orange bars) highlights the number of successful fits obtained with each growth rate. The modal growth rate is 2×10^{-11} m/s (n = 15), which provided a best-fit model in 25% of the initial model runs. To aid comparison of diffusion timescales between crystals and samples, models were subsequently re-run using a fixed growth rate of 2×10^{-11} m/s to determine the diffusion timescales reported in Table 2. Details of the diffusion profiles, input parameters, and timescales for the initial model runs prior to using a fixed growth rate of 2×10^{-11} m/s are reported for completeness in the Supplementary Material.

of Apollo mare basalts include 3.1623×10^{-11} m/s (Borell and Kilinc, 2012) used by Neal et al. (2015) and Bell et al. (2020), and 1.5×10^{-12} m/s (Vinet and Higgins, 2010) used by Donohue and Neal (2015). Crystal size distribution analysis of the low-Ti LaPaz group and Northwest Africa (NWA) 032 mare basalt meteorites by Day and Taylor (2007) used olivine growth rates of 5.4×10^{-12} m/s (Cashman and Marsh, 1988). Richter et al. (2021) report growth rates of $\sim 5.6 \times 10^{-11}$ m/s following Fe-Mg interdiffusion and isotopic fractionation studies of olivine in Apollo 15 basalt 15555. The olivine crystal growth rate of 2×10^{-11} m/s used to fit diffusion models in this study therefore lies within the range of olivine growth rates previously used in lunar and terrestrial literature for basaltic samples.

5.3. Diffusion model variables – Cooling rate

Numerous experimental petrological studies were conducted on synthetic analogues of the Apollo 15 samples in the mid to late 1970 s to determine the cooling rates of the quartz-normative and olivine-normative basalts (Lofgren et al., 1974, 1975; Taylor et al., 1975; Bianco and Taylor, 1977; Grove and Bence, 1977; Grove and Walker, 1977; Taylor et al., 1977). The textures and chemistries of the experimental samples were compared to the natural samples to determine a range of cooling rates applicable to the Apollo 15 mare basalts. These reported cooling rates range from 0.01 to >100 °C/hr, with the majority studies reporting cooling rates in the region of <30 °C/hr (Lofgren et al., 1974, 1975; Bianco and Taylor, 1977; Grove and Walker, 1977; Taylor et al., 1977; Grove, 1982). Lofgren et al. (1975) and Grove and Walker (1977) determined experimental cooling rates for samples 15125 and 15485, two quartz-normative basalts that were also included in our study. Lofgren et al. (1975) concluded that 15125 cooled at 2–5 °C/hr and 15485 cooled at a faster rate of 5–20 °C/hr. The cooling rates calculated by Grove and Walker (1977) are of the same order of magnitude: they determined that 15485 had a slower cooling rate of 3.75–10 °C/hr than 15125 at 10–30 °C/hr. In both cases, the cooling rates calculated by experimental petrology are faster than those used in our diffusion models, which ranged from 0.5 to 0.8 °C/hr for olivine crystals in 15125 and 0.35–0.6 °C/hr for 15485. There are similar differences for sample 15555, where experimental cooling rates have been determined at 0.5–1 °C/hr (Bianco and Taylor, 1977), while cooling rates of 0.04–0.1 °C/hr provided the best fit in our diffusion modelling.

Our study is not the first to document that experimentally derived cooling rates for Apollo 15 samples are faster than those determined via diffusion modelling. Taylor et al. (1977) and Richter et al. (2021) both modelled Fe-Mg interdiffusion in an olivine crystal from sample 15555 and calculated a cooling rate of 0.2 °C/hr. Walker et al. (1977) also used diffusion equations for Fe-Mg in olivine to calculate a similar cooling rate of ~0.16 °C/hr for 15555. It is important to note that each study used different diffusivity parameterisations. Whilst our cooling rates of 0.04–0.1 °C/hr for 15555 falls within the range reported in previous studies, corrections to the diffusivity parameters would need to be able to compare them directly. This is particularly significant when comparing some of the original studies (Taylor et al., 1977; Walker et al., 1977) to more recent studies which use updated and better-defined values for diffusivity (Richter et al., 2021). Walker et al. (1977) suggested that cooling rates may be faster in experimental crystallisation studies as they are limited by constraints such as the size of the vessel and are not able to accurately recreate coarse-grained textures that can be directly compared with natural coarse-grained samples or phenocrysts. As such, the difference between the cooling rates calculated by experimental methods and those determined in our study could be at least partly attributed to the limitations of different methods.

5.4. Origin of the compositional zoning

The olivine zoning patterns and short diffusion timescales in the olivine-normative and quartz-normative basalts most likely formed during the final stages of cooling within surficial lava flows. This is consistent with the rapid crystal rim growth rates needed to obtain successful diffusion model fits to the compositional data (Figs. 3 and 6). We suggest that the olivine cores likely crystallised from magma in the subsurface prior to eruption, followed by low-Fo rim crystallisation in the stagnating lava flow, from residual pockets of melt. This is consistent

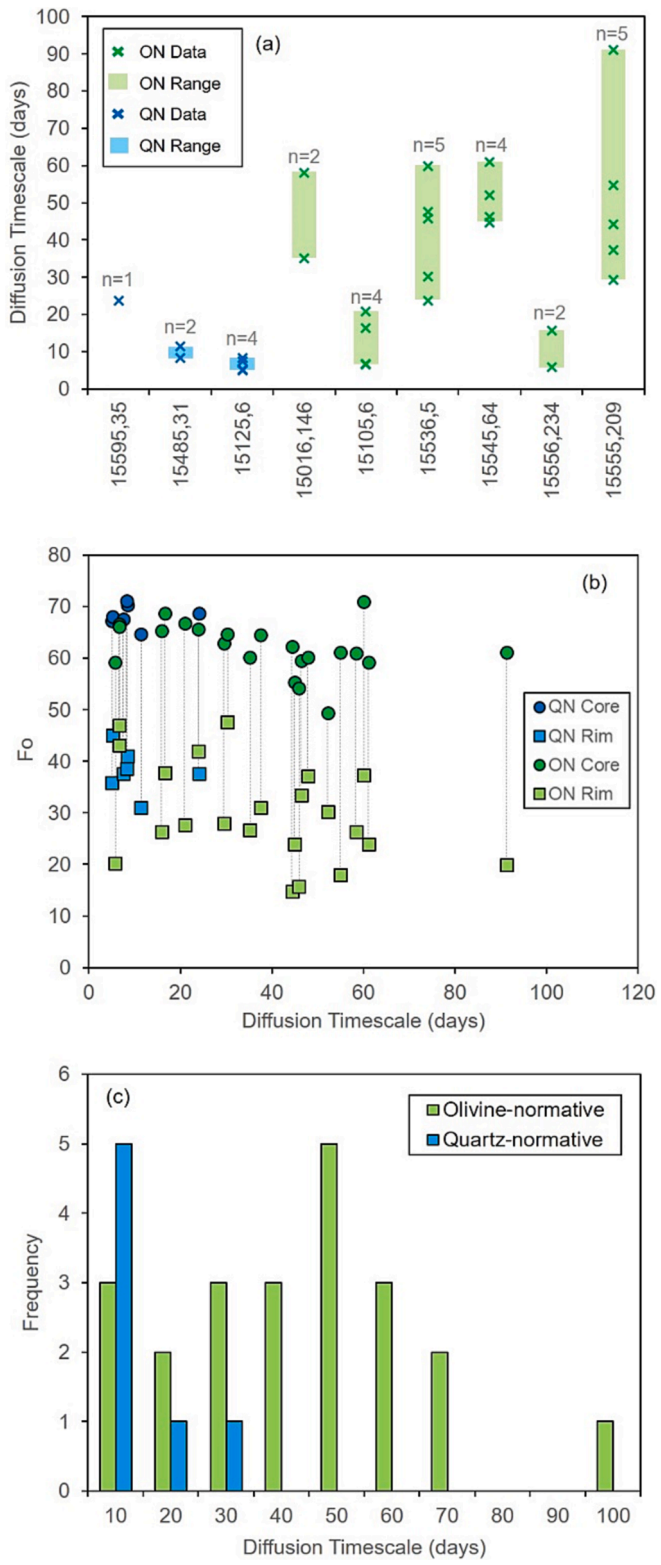

Fig. 6. (a) Diffusion timescales for individual crystals, and timescale ranges for each sample (n = number of crystals per sample). (b) Diffusion timescales plotted against olivine core and rim compositions with tie lines linking core and rim values. (c) Frequency of diffusion timescales for both suites.

with the textural characteristics of the samples, particularly the olivine-normative basalts, which show olivine phenocrysts with low-Fo rims that appear to grow into the interstitial space between adjacent crystals, such that low-Fo rims are not perfectly concentric (Fig. 3a). Likewise, the lowest-Fo rims are often found in conjunction with areas of late-stage mesostasis (Fig. 3a).

One of the potential outcomes of this study was to explore how diffusion modelling can be used to gain a further understanding of the petrogenesis, thermal histories and relationship between the olivine- and quartz-normative basalts. The model proposed by Schnare et al. (2008) suggests that the quartz-normative basalts may have experienced a complex magmatic history involving storage and fractionation in magma chambers within the lunar crust, while the olivine-normative basalts crystallized primarily in lava flows at the lunar surface. In this scenario, we might expect quartz-normative basalts to contain zoned olivine crystals with longer diffusion timescales that preserve records of magma crystallisation and storage within the lunar crust prior to eruption. If such a plumbing system was in operation, then we might also expect to observe reverse or oscillatory zoning in some olivine crystals in quartz-normative samples due to processes of magma mixing and/or the replenishment of a magma chamber/s (e.g., Elardo and Shearer, 2014; Rae et al., 2016; Viccaro et al., 2016; Kahl et al., 2017; Gordeychik et al., 2018; Giuffrida et al., 2020). By contrast, we might expect the olivine-normative basalts to contain only simply zoned olivines and to record shorter timescales reflecting faster cooling on the lunar surface. We found only normal zoning in the olivine crystals from both the quartz-normative and olivine-normative samples. Additionally, the diffusion timescales for the quartz-normative samples are slightly shorter (5–24 days) than the olivine-normative basalts (6–91 days). At face value, these timescales suggest that the quartz-normative and olivine-normative basalts experienced similar thermal histories. We did not find any complex-zoned olivine crystals or long diffusion timescales consistent with complex thermal and crystallisation histories in different magmatic environments, although we cannot exclude the possibility that such crystals did form, but were not transported to the lunar surface. We note that the MELTS modelling of olivine crystallisation from quartz-normative sample bulk chemistries (Table 1) did not predict the high-Fo olivine cores found in the samples (Fig. 2). This could potentially indicate that there were two periods of crystallisation: the first in a high-Fo mafic system, followed by a second in a low-Fo evolved system. In this scenario, it is possible that the high-Fo olivine cores in the quartz-normative samples were inherited via crystal entrainment or magma mixing, although we are not able to place constraints on the potential source(s) of the high-Fo olivine cores. In studies of mare basalt meteorite LaPaz Icefield 02205, higher-Mg olivine cores of $>Fo_{54}$ were also not predicted by MELTS modelling despite olivine with cores of Fo_{64} present within the sample (Anand et al., 2006). In this case, it was suggested that the high-Mg olivine cores could be xenocrystic (Anand et al., 2006; Joy et al., 2006). Schnare et al. (2008), also suggest that entrained olivine is possible in the quartz-normative basalts in the form of cumulus olivine from magma ponded at crustal levels. Texturally, the olivine phenocrysts in the quartz-normative samples in this study are small and so their size is not necessarily indicative of entrained crystals.

5.5. *Using diffusion timescales to calculate lava flow thickness*

We interpret that our Apollo 15 basalt calculated diffusion timescales (Table 2) represent time spent cooling within a lava flow. As such, we are able to use the timescales to calculate an estimate of the minimum lava flow thicknesses of both suites of basalts at the Apollo 15 landing site.

Jaeger (1961) developed equations to model the cooling of an extrusive lava sheet that loses latent heat through crystallisation and via conductive heat transfer to the country rock. The equations allow the temperature of a lava flow to be calculated at any given time after emplacement. Isotherms can also be calculated for the flow interior of any given thickness if the dimensionless value τ is used instead of time (Lovering, 1935; Jaeger, 1961). The value τ is proportional to time after emplacement (t) and is defined by the equation:

$$\tau = kt/d^2 \quad (1)$$

where d is the thickness of the lava flow and k is the thermal diffusivity. The thermal diffusivity (k) of a lava flow can be calculated from the thermal conductivity (K), density (ρ), and the specific heat (c) in the equation:

$$k = K/\rho c \quad (2)$$

The values used to calculate the thermal diffusivity of low-Ti Apollo 15 samples in this study (and for lunar basaltic lava flows more generally) are a thermal conductivity of 0.67 W m^{-1} K^{-1} (Rumpf et al., 2013), a specific heat of 1100 J Kg^{-1} K^{-1} (Rumpf et al., 2013), and a low-Ti mare basalt density of 2950 kg m^{-3} (Wieczorek et al., 2006). Using Eq. (2), the resulting thermal diffusivity is 4.78 m^2 per year.

The temperature (T) of a lava flow at a given depth (d) at any given time (t) can be calculated using the equation:

$$T/T_0 = \frac{1}{2}\left\{erf\frac{y+d}{2d\tau^{\frac{1}{2}}} + erf\frac{y-d}{2d\tau^{\frac{1}{2}}} - 2erf\frac{y}{2d\tau^{\frac{1}{2}}}\right\} \quad (3)$$

where T_0 is the lava temperature at the moment of emplacement, *erf* is the error function, y is the vertical distance from the lava upper surface and τ is dimensionless time as defined in Eq. (1). Eq. (3) assumes the temperature of the upper surface of the lava and the country rock are fixed at zero, and that the lava temperature at the moment of emplacement (T_0) is invariant with depth (Jaeger, 1961). As detailed in model runs by Jaeger (1961), the addition of rapid cooling via radiant loss of heat through the upper surface of a lava flow has a negligible impact on this calculation, and so an assumed upper surface temperature of zero is sufficient.

Diffusion timescale values were used to calculate minimum lava flow thicknesses for the olivine-normative and quartz-normative suites at the Apollo 15 landing site. Iterative calculations were made by using Eq. (3) and incrementally increasing the lava flow depth in intervals of 0.5 m from 0.5 m to 11 m. The minimum lava flow thickness is identified when the peak temperature within the flow is equal to the end temperature (T_t) reported in the diffusion modelling (Fig. 7b). The calculation was repeated using the individual diffusion timescales for each olivine crystals as a fixed value for time, and the individual diffusion modelling start temperature as a fixed T_0 value (Table 2).

Calculated minimum lava flow thicknesses using individual olivine crystal diffusion timescales from olivine-normative samples range from 2 to 6 m with an average of 4 m (Fig. 7). Individual olivine crystal diffusion timescales from quartz-normative samples yielded thinner minimum flow depths of 1.5–3 m with an average of 2 m (Fig. 7). As such, to accommodate all the individual crystal results in this study a minimum lava flow thickness of 6 m would be required for the olivine-normative samples, and a minimum flow thickness of 3 m for the quartz-normative samples. The difference between the two suites is reflective of the difference in diffusion timescales. The longer diffusion timescales of

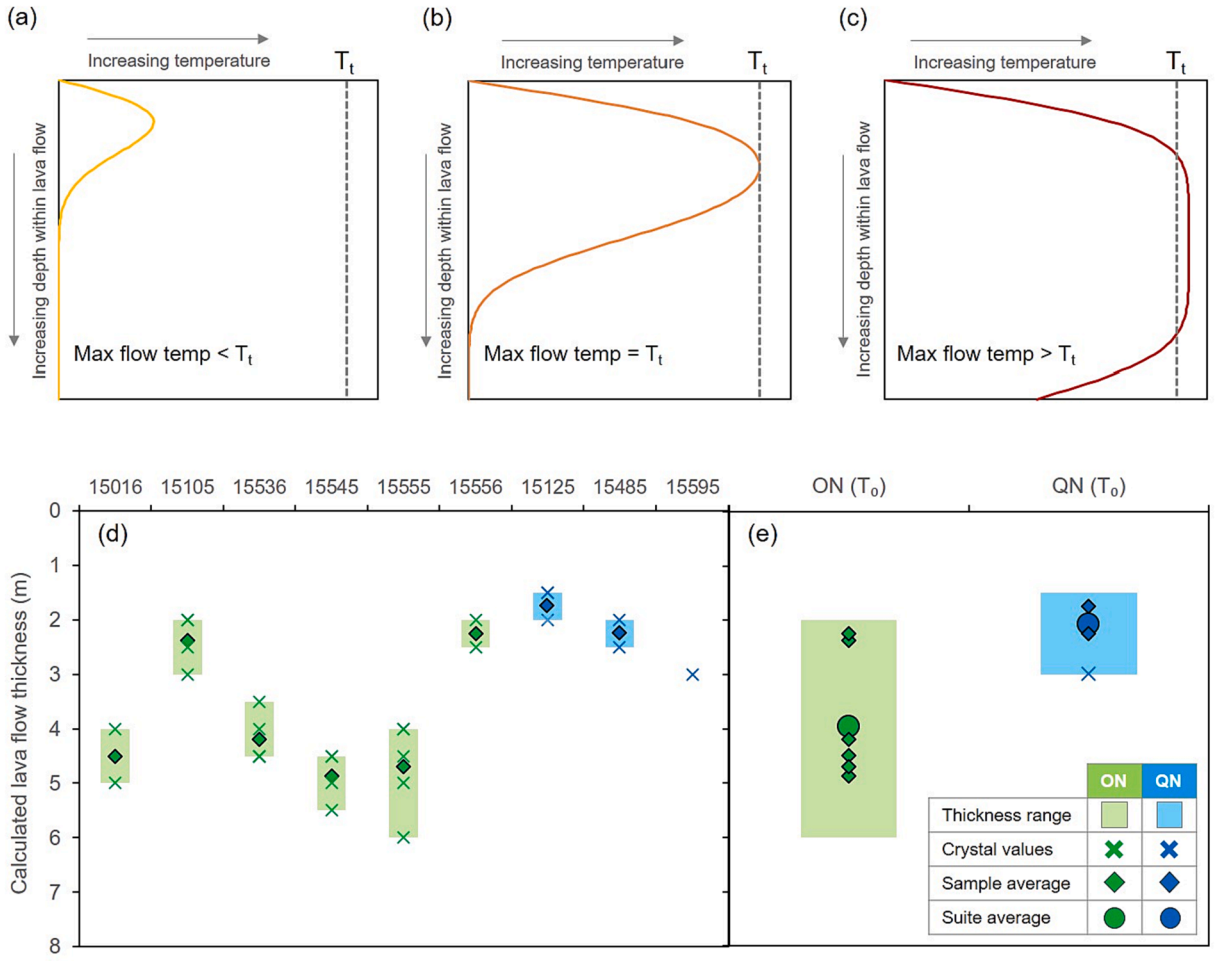

Fig. 7. (a–c) Schematic plots showing how flow thickness was varied until the maximum flow temperature was equal to T_t (b) after the given time (i.e., diffusion timescale) using the equations from Jaeger (1961). In (a), the lava has cooled below T_t after the time given by the Fe-Mg interdiffusion timescale and is therefore too thin. In (c), the lava core is hotter than T_t after the time given by the Fe-Mg interdiffusion timescales and is, therefore, too thick. Note that the upper and lower parts of the lava have cooled below T_t. (d) A summary of the flow thickness values for each sample, including the range in values for each individual crystal. (e) A summary of the range of lava flow thicknesses for each suite. ON = olivine-normative (shown in green), QN = quartz-normative (shown in blue).

the olivine-normative samples mean that thicker lava flows are needed to maintain a (comparatively similar) temperature equal to T_t after the defined period of time, compared with the quartz-normative samples.

Previous, predominantly experimental, studies of the Apollo 15 mare basalts have yielded a range of estimated thicknesses for the quartz-normative and olivine-normative lava flows. Grove and Walker (1977) used synthetic analogues of sample 15597 to determine that the coarsest grained quartz-normative basalts (not analysed in this study) cooled at least 10 m away from a flow contact with a likely lava flow thickness of 20 m. Lofgren et al. (1975) also compared Apollo 15 sample textures to experimentally cooled analogues and concluded that the quartz-normative basalts are from a 2–3 m-thick lava flow. On the other hand, Takeda et al. (1975) used cooling rates determined by the degree of exsolution in pyroxene crystals to calculate a general lava flow thickness of 4–10 m for the Apollo 15 mare basalts, with a lava flow depth of 6 m being able to accommodate a range in cooling rates from 0.16 to 12 °C/hr. Our calculated minimum lava flow thicknesses are, therefore, consistent with these previous studies.

Unique to the Apollo 15 landing site, astronauts were able to take images of outcrops of lava flows exposed within the slopes of Hadley Rille, a collapsed lava tube to the west of the landing site (Fig. 8). Images of the western side of Hadley Rille show bedrock exposed in the top 35–60 m of the rille walls, which are located above 300 m of rocky talus that leads down to the base of the rille (ALGIT, 1972; Swann et al., 1972). The rock exposures can be split into three intervals (Fig. 8): a lower thinly layered 8–16 m portion with at least 12 identifiable layers up to 1–3 m thick; a massive middle portion 10–20 m thick; and a thin, poorly exposed, darker unit at the top (ALGIT, 1972; Howard et al., 1972; Swann et al., 1972). It has been determined from geological field relationships, crater excavation depths and radiometric age dating that the olivine-normative basalts are stratigraphically above the quartz-normative basalts (ALGIT, 1972), but correlations between the sampling localities east of the rille and the outcrops photographed in the western wall of the rille remain uncertain (Howard et al., 1972). Our results suggest thicker olivine-normative flows with a minimum thickness of 6 m and thinner quartz-normative flows with a minimum thickness of 3 m. We therefore speculate that the olivine-normative samples (erupted at 3287 ± 21 Ma) could correspond to the photographed upper massive units, and the quartz-normative samples (erupted at 3371 ± 21 Ma) could correspond to the lower thinly bedded units.

The Apollo 15 samples provided a unique opportunity to test diffusion modelling derived lava flow thickness estimates against outcrop observations made in the field at the Apollo 15 landing site in the walls of Hadley Rille (Howard et al., 1972). Our modelled timescales correspond to the period of time the olivine crystals spent cooling within the lava flow – that is, the period between the onset of rim growth and final solidification. Our results indicate that the olivine-normative and quartz-normative basalts were emplaced by similar eruption and lava flow processes at the Apollo 15 landing site, despite the ~100 Myr difference in their average eruption ages (Snape et al., 2019). Two out of the six olivine-normative samples show similar diffusion timescales to the quartz-normative samples, and the diffusion timescales for the dataset as a whole are all in the order of <100 days. The only difference we can interpret from our modelled diffusion timescales and subsequent calculated lava flow thicknesses is that the olivine-normative lava flows at the Apollo 15 landing site are thicker (>6 m) than the quartz-normative lava flows (>3 m). This may be due to a larger volume of material having been erupted during the olivine-normative basalt eruption, possibly in more sustained eruptions compared with the thinner quartz-normative lava flows. However, as we are only seeing a snapshot of the field relationships in the walls of Hadley Rille (Fig. 8), the larger relative thickness of the olivine-normative lava flows could also be due to factors such as the underlying topography or the proximity to the eruption source. Our results demonstrate that diffusion timescales can be used to independently constrain lunar lava flow thicknesses, providing a new method of determining minimum thickness of individual flow units in cases where diffusion is thought to occur during cooling within a lava flow. This method is particularly suited to precious lunar samples because the analysis is non-destructive. The method can be applied to rock samples for which field relationships may

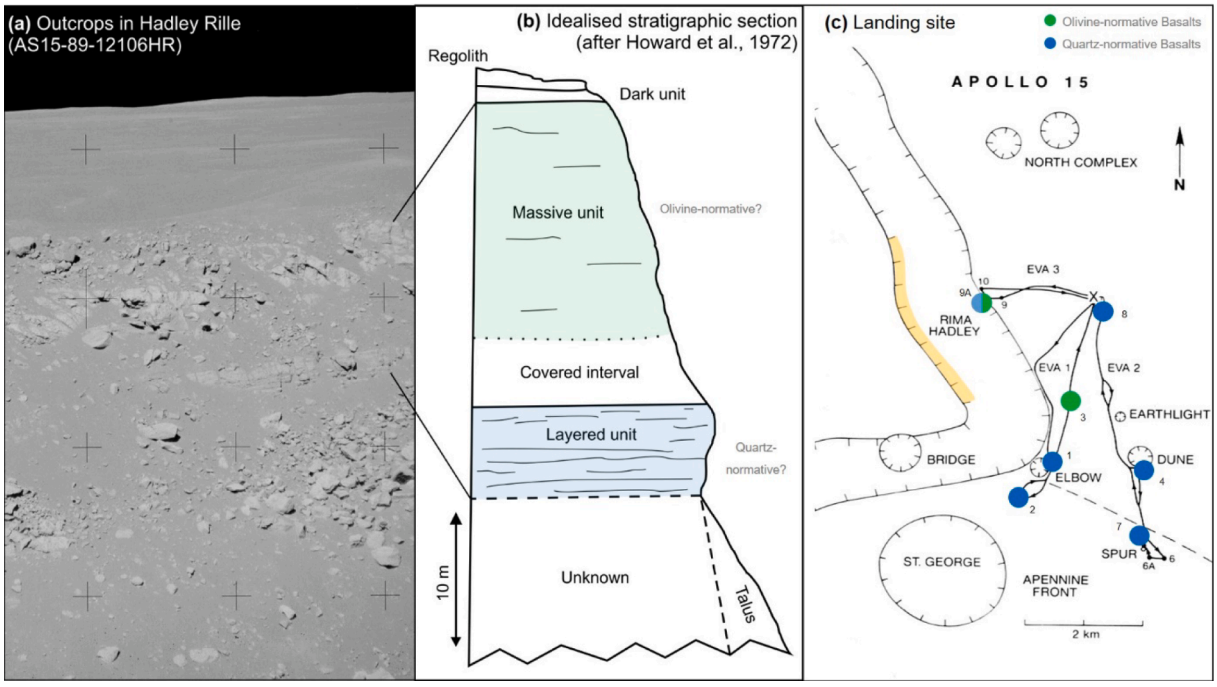

Fig. 8. (a) Photograph of the outcrops in Hadley Rille taken by the Apollo 15 astronauts from the eastern side of the rille at station 10 (NASA image: AS15-89-12106HR). (b) An idealised stratigraphic section shows three distinct intervals within the upper regions of the rille walls, including a massive unit lying stratigraphically above a thinner layered unit (after Howard et al., 1972). (c) Map of the Apollo 15 landing site (after LPI, 2017) showing the three EVA (extravehicular activity) traverses and associated sampling stations. Stations at which samples (>20 g) of olivine normative (green) and quartz-normative (blue) basalts are shown for reference. The western wall of Hadley Rille (Rima Hadley), a portion of which is shown in (a), is highlighted in yellow.

be uncertain. As such, diffusion modelling of olivine could be potentially used to provide estimates of lava flow thicknesses at other Apollo landing sites and at future lunar landing site locations where bedrock exposures of mare basalt lava flows may not be visible. Estimates of individual lava flow thicknesses for mare regions across the lunar surface erupted at various points in time during the thermal evolution of the Moon would help to build a more detailed understanding of lunar volcanic flux and eruption styles. Such data would be of use to models of transient lunar atmospheres and the origin of lunar volatiles (e.g. Needham and Kring, 2017), which are currently high priority lunar and planetary science goals (NRC, 2007; National Academies of Sciences, Engineering, and Medicine, 2022). More widely, the approach of using olivine diffusion modelling to constrain lava flow cooling rates could potentially be used to calculate lava flow thickness of other types of olivine-bearing basalts such as martian shergottites (e.g. McCoy and Lofgren, 1999; First and Hammer, 2016), asteroidal angrites and eucrites (Hayashi et al., 2020), helping to shed light on the comparative volcanic history of planetary basalts across the inner Solar System (e.g. Basaltic Volcanism Study Project, 1981).

6. Conclusion

We conducted Fe-Mg interdiffusion modelling for olivine crystals from quartz-normative and olivine-normative Apollo 15 mare basalts. We used a dynamic model that accounts for the effects of growth and changing boundary conditions of the crystals, meaning that valuable information can be gathered from crystals that cannot be accurately modelled using simple isothermal diffusion models. In summary, our work shows:

- Quartz-normative diffusion timescales range from 5 to 24 days and olivine-normative samples from 6 to 91 days and likely record the final stages of cooling within a lava flow on the lunar surface.
- Similarities in calculated diffusion timescales between the two suites suggesting that the quartz-normative and olivine-normative basalts experienced similar thermal histories. This does not appear to support the theory that the two suites may have experienced different thermal and crystallisation histories in the lunar crust, as proposed in some petrogenetic models (e.g., Schnare et al., 2008). Although we note that our results do not exclude the possibility that complex crystal archives were formed at these volcanic centres, but were simply not erupted to the surface.
- We combined our calculated diffusion timescales with a conductive cooling model (Jaeger, 1961), to derive minimum lava flow thickness estimates of 6 m for olivine-normative basalts and 3 m for quartz-normative basalts.
- The range in minimum lava flow thicknesses agree with previous estimates in the literature and with the thickness of outcrops observed in the walls of Hadley Rille by the Apollo 15 crew (Howard et al., 1972) (Fig. 8).

Modelling of Fe-Mg interdiffusion in olivine, as well as diffusion in other minerals, enables a large amount of information to be gathered from individual crystals within a sample. This is undoubtedly a valuable tool that could be utilised to gain additional insight into lunar magmatic systems and volcanic processes from other Apollo samples, lunar meteorites, and future lunar sample return samples where field observations may be limited.

CRediT authorship contribution statement

S.K. Bell: Writing – original draft, Investigation, Conceptualization. **D.J. Morgan:** Methodology, Conceptualization, Writing – review & editing. **K.H. Joy:** Writing – review & editing, Conceptualization, Supervision. **J.F. Pernet-Fisher:** Writing – review & editing, Conceptualization, Supervision. **M.E. Hartley:** Writing – review & editing, Conceptualization, Supervision.

Declaration of Competing Interest

The authors declare that they have no known competing financial interests or personal relationships that could have appeared to influence the work reported in this paper.

Acknowledgements

We thank Stuart Kearns for his assistance with EPMA analyses, and Ali Gholina for assistance with EBSD analyses. For the provision and preparation of Apollo samples we thank the NASA Johnson Space Center curatorial team. This work was supported by a Science and Technology Facilities Council studentship to SB (Award Ref: 1799244), a Royal Society University Research Fellowship (URF\R\201009) and Science and Technology Facilities Council grant (ST/V000675/1) to KHJ. We thank Bernard Charlier for editorial handling, and Helena Albert and two anonymous reviewers for their constructive and helpful comments.

Appendix A. Supplementary material

Supplementary Data file 1 is a PDF containing supplementary Figs. S1–S21. Supplementary Data file 2 is a spreadsheet containing the raw numerical values used to produce the figures included in the main manuscript, as well as full EPMA and EBSD data for each sample. Supplementary material to this article can be found online at https://doi.org/10.1016/j.gca.2023.08.009.

References

Abràmoff, M.D., Magalhães, P.J., Ram, S.J., 2004. Image processing with ImageJ. Biophoton. Int. 11 (7), 36–42.
ALGIT (Apollo Lunar Geology Investigation Team), 1972. Geologic setting of the Apollo 15 samples. Science 175 (4020), 407–415.
Allan, A.S., Morgan, D.J., Wilson, C.J., Millet, M.A., 2013. From mush to eruption in centuries: Assembly of the super-sized Oruanui magma body. Contrib. Mineral. Pet. 166 (1), 143–164.
Anand, M., Taylor, L.A., Misra, K.C., Demidova, S.I., Nazarov, M.A., 2003. KREEPy lunar meteorite Dhofar 287A: A new lunar mare basalt. MaPS 38 (4), 485–499.
Anand, M., Taylor, L.A., Floss, C., Neal, C.R., Terada, K., Tanikawa, S., 2006. Petrology and geochemistry of LaPaz Icefield 02205: A new unique low-Ti mare-basalt meteorite. GCA 70 (1), 246–264.
Basaltic Volcanism Study Project, 1981. Basaltic Volcanism on the Terrestrial Planets. Pergamon Press Inc, New York, pp. 1–1286.
Bell, S.K., Joy, K.H., Pernet-Fisher, J.F., Hartley, M.E., 2020. QEMSCAN as a method of semi-automated crystal size distribution analysis: Insights from Apollo 15 mare basalts. J. Petrol. 61 (4).
Bell, S.K., Joy, K.H., Pernet-Fisher, J.F., Hartley, M.E., 2023. Investigating the crystallization history of Apollo 15 mare basalts using quantitative textural analysis. MaPS 58 (7), 955–977.
Bianco, A.S., Taylor, L.A., 1977. Applications of dynamic crystallization studies-lunar olivine-normative basalts. In: 8th Lunar Sci. Conf. Proc., pp. 1593–1610.
Borell, A., Kilinc, A., 2012. Growth rate of olivine in a basaltic melt from the Kilauea volcano in Hawaii using crystal size distribution theory. Geol. Soc. Am. Bull. 44 (7), 560.
Brett, R., 1975. Thickness of some lunar basalt flows and ejecta blankets based on chemical kinetic data. GCA 39, 1135–1141.
Cashman, K.V., Marsh, B.D., 1988. Crystal size distribution (CSD) in rocks and the kinetics and dynamics of crystallization II: Makaopuhi lava lake. Contrib. Mineral. Pet. 99 (3), 292–305.
Chappell, B.W., Green, D.H., 1973. Chemical compositions and petrogenetic relationships in Apollo 15 mare basalts. EPSL 18 (2), 237–246.
Chappell, B.W., Compston, W., Green, D.H., Ware, N.G., 1972. Chemistry, geochronology and petrogenesis of lunar sample 15555. Science 175, 415–416.
Costa, F., Chakraborty, S., 2004. Decadal time gaps between mafic intrusion and silicic eruption obtained from chemical zoning patterns in olivine. EPSL 227 (3–4), 517–530.
Costa, F., Morgan, D., 2010. Time Constraints from Chemical Equilibration in Magmatic Crystals. Timescales of Magmatic Processes: From Core to Atmosphere. Wiley, Chichester, pp. 125–159.
Costa, F., Dohmen, R., Chakraborty, S., 2008. Time scales of magmatic processes from modelling the zoning patterns of crystals. Rev. Mineral. Geochem. 69 (1), 545–594.
Couperthwaite, F.K., Thordarson, T., Morgan, D.J., Harvey, J., Wilson, M., 2020. Diffusion timescales of magmatic processes in the Moinui lava eruption at Mauna Loa, Hawaii, as inferred from bimodal olivine populations. J. Petrol. 61 (7).

Couperthwaite, F.K., Morgan, D., Pankhurst, M.J., Lee, P.D., Day, J.M.D., 2021. Reducing epistemic and model uncertainty in ionic inter-diffusion chronology: A 3D observation and dynamic modelling approach using olivine from Piton de la Fournaise, La Réunion. Am. Mineral. 106 (3), 481–494.
Day, J., Taylor, L.A., 2007. On the structure of mare basalt lava flows from textural analysis of the LaPaz Icefield and Northwest Africa 032 lunar meteorites. MaPS 42 (1), 3–17.
Dohmen, R., Becker, H.W., Chakraborty, S., 2007. Fe–Mg diffusion in olivine I: Experimental determination between 700 and 1,200 C as a function of composition, crystal orientation and oxygen fugacity. Phys. Chem. Miner. 34 (6), 389–407.
Dohmen, R., Chakraborty, S., 2007. Fe–Mg diffusion in olivine II: Point defect chemistry, change of diffusion mechanisms and a model for calculation of diffusion coefficients in natural olivine. Phys. Chem. Miner. 34 (6), 409–430.
Donohue, P.H., Neal, C.R., 2015. Quantitative textural analysis of ilmenite in Apollo 17 high-titanium mare basalts. GCA 149, 115–130.
Dowty, E., Prinz, M., Keil, K., 1973. Composition, mineralogy, and petrology of 28 mare basalts from Apollo 15 rake samples. In: 4th Lunar Sci. Conf. Proc., pp.423–444.
Du, J., Fa, W., Wieczorek, M.A., Xie, M., Cai, Y., Zhu, M.H., 2019. Thickness of lunar mare basalts: New results based on modeling the degradation of partially buried craters. J. Geophys. Res. Planets 124 (9), 2430–2459.
Duncan, A.R., Erlank, A.J., Sher, M.K., Abraham, Y.C., Willis, J.P., Ahrens, L.H., 1976. Some trace element constraints on lunar basalt petrogenesis. In: 7th Lunar Sci. Conf. Proc., pp. 1659–1671.
Elardo, S.M., Shearer Jr, C.K., 2014. Magma chamber dynamics recorded by oscillatory zoning in pyroxene and olivine phenocrysts in basaltic lunar meteorite Northwest Africa 032. Am. Mineral. 99 (2–3), 355–368.
First, E., Hammer, J., 2016. Igneous cooling history of olivine-phyric shergottite Yamato 980459 constrained by dynamic crystallization experiments. MaPS 51 (7), 1233–1255.
Garry, W.B., Robinson, M.S., Zimbelman, J.R., Bleacher, J.E., Hawke, B.R., Crumpler, L. S., Braden, S.E., Sato, H., 2012. The origin of Ina: Evidence for inflated lava flows on the Moon. J. Geophys. Res.: Planets 117, E00H31.
Ghiorso, M.S., Gualda, G.A., 2015. An H_2O–CO_2 mixed fluid saturation model compatible with rhyolite-MELTS. Contrib. Mineral. Petrol. 169 (6), 1–30.
Gifford, A.W., El-Baz, F., 1981. Thicknesses of lunar mare flow fronts. Moon Planets 24 (4), 391–398.
Girona, T., Costa, F., 2013. DIPRA: A user-friendly program to model multi-element diffusion in olivine with applications to timescales of magmatic processes. Geochem. Geophys. Geosyst. 14 (2), 422–431.
Giuffrida, M., Nicotra, E., Viccaro, M., 2020. Changing modes and rates of mafic magma supply at Pantelleria (Sicily Channel, Southern Italy): New perspectives on the volcano factory drawn upon olivine records. J. Petrol. 61 (5).
Gong, S., Wieczorek, M.A., Nimmo, F., Kiefer, W.S., Head, J.W., Huang, C., Smith, D.E., Zuber, M.T., 2016. Thicknesses of mare basalts on the Moon from gravity and topography. J. Geophys. Res. Planets 121 (5), 854–870.
Gordeychik, B., Churikova, T., Kronz, A., Sundermeyer, C., Simakin, A., Wörner, G., 2018. Growth of, and diffusion in, olivine in ultra-fast ascending basalt magmas from Shiveluch volcano. Sci. Rep. 8 (1), 1–15.
Grove, T.L., 1982. Use of exsolution lamellae in lunar clinopyroxenes as cooling rate speedometers: An experimental calibration. Am. Mineral. 67 (3–4), 251–268.
Grove, T.L., Bence, A.E., 1977. Experimental study of pyroxene-liquid interaction in quartz-normative basalt 15597. In: 8th Lunar Sci. Conf. Proc., pp. 1549–1579.
Grove, T.L., Walker, D., 1977. Cooling histories of Apollo 15 quartz-normative basalts. In: 8th Lunar Sci. Conf. Proc., pp. 1501–1520.
Gualda, G.A.R., Ghiorso, M.S., Lemons, R.V., Carley, T.L., 2012. Rhyolite-MELTS: A modified calibration of MELTS optimized for silica-rich, fluid-bearing magmatic systems. J. Petrol. 53, 875–890.
Hallis, L.J., Anand, M., Strekopytov, S., 2014. Trace-element modelling of mare basalt parental melts: Implications for a heterogeneous lunar mantle. GCA 134, 289–316.
Hartley, M.E., Morgan, D.J., Maclennan, J., Edmonds, M., Thordarson, T., 2016. Tracking timescales of short-term precursors to large basaltic fissure eruptions through Fe–Mg diffusion in olivine. EPSL 439, 58–70.
Hayashi, H., Mikouchi, T., Yamaguchi, A., 2020. Olivine xenocrysts and cooling rates of quenched angrites: Implications for the stratigraphy of their igneous body. In: 11th Symp. on Polar Science, pp. 1–2.
Hiesinger, H., Head III, J.W., Wolf, U., Jaumann, R., Neukum, G., 2002. Lunar mare basalt flow units: Thicknesses determined from crater size-frequency distributions. Geophys. Res. Lett. 29 (8), 89–181.
Howard, K.A., Head, J.W., Swann, G.A., 1972. Geology of Hadley Rille. In: 3rd Lunar Sci. Conf. Proc., pp. 1-14.
Ishiyama, K., Kumamoto, A., Ono, T., Yamaguchi, Y., Haruyama, J., Ohtake, M., Katoh, Y., Terada, N., Oshigami, S., 2013. Estimation of the permittivity and porosity of the lunar uppermost basalt layer based on observations of impact craters by SELENE. J. Geophys. Res. Planets 118 (7), 1453–1467.
Jaeger, J.C., 1961. The cooling of irregularly shaped igneous bodies. Am. J. Sci. 259 (10), 721–734.
Joy, K.H., Crawford, I.A., Downes, H., Russell, S.S., Kearsley, A.T., 2006. A petrological, mineralogical, and chemical analysis of the lunar mare basalt meteorite LaPaz Icefield 02205, 02224, and 02226. MaPS 41 (7), 1003–1025.
Kahl, M., Chakraborty, S., Costa, F., Pompilio, M., 2011. Dynamic plumbing system beneath volcanoes revealed by kinetic modelling, and the connection to monitoring data: An example from Mt. Etna. EPSL 308 (1–2), 11–22.
Kahl, M., Chakraborty, S., Costa, F., Pompilio, M., Liuzzo, M., Viccaro, M., 2013. Compositionally zoned crystals and real-time degassing data reveal changes in magma transfer dynamics during the 2006 summit eruptive episodes of Mt. Etna. Bull. Volcanol. 75 (2), 692.
Kahl, M., Chakraborty, S., Pompilio, M., Costa, F., 2015. Constraints on the nature and evolution of the magma plumbing system of Mt. Etna volcano (1991–2008) from a combined thermodynamic and kinetic modelling of the compositional record of minerals. J. Petrol. 56 (10), 2025–2068.
Kahl, M., Viccaro, M., Ubide, T., Morgan, D.J., Dingwell, D.B., 2017. A branched magma feeder system during the 1669 eruption of Mt Etna: Evidence from a time-integrated study of zoned olivine phenocryst populations. J. Petrol. 58 (3), 443–472.
Lai, J., Xu, Y., Bugiolacchi, R., Meng, X., Xiao, L., Xie, M., Liu, B., Di, K., Zhang, X., Zhou, B., Shen, S., 2020. First look by the Yutu-2 rover at the deep subsurface structure at the lunar farside. Nature Commun. 11 (1), 3426.
Li, S., Hsu, W., Guan, Y., Wang, L., Wang, Y., 2016. Petrogenesis of the Northwest Africa 4898 high-Al mare basalt. MaPS 51 (7), 1268–1288.
Lindstrom, M.M., Haskin, L.A., 1978. Causes of compositional variations within mare basalt suites. In: 9th Lunar Sci. Conf. Proc., pp. 465–486.
Lofgren, G., Donaldson, C.H., Williams, R.J., Mullins Jr, O., Usselman, T.M., 1974. Experimentally reproduced textures and mineral chemistry of Apollo 15 quartz normative basalts. In: 5th Lunar Sci. Conf. Proc., pp. 549–567.
Lofgren, G.E., Donaldson, C.H., Usselman, T.M., 1975. Geology, petrology, and crystallization of Apollo 15 quartz-normative basalts. In: 6th Lunar Sci. Conf. Proc., pp. 79–99.
Lovering, T.S., 1935. Theory of heat conduction applied to geological problems. Bulletin Geol. Soc. Am. 46 (1), 69–94.
Ma, M.S., Murali, A.V., Schmitt, R.A., 1976. Chemical constraints for mare basalt genesis. In: 7th Lunar Sci. Conf. Proc., pp. 1673–1695.
Ma, M.S., Schmitt, R.A., Warner, R.D., Taylor, G.J., Keil, K., 1978. Genesis of Apollo 15 olivine normative mare basalts-Trace element correlations. In: 9th Lunar Sci. Conf. Proc., pp. 523–533.
Mason, B., Jarosewich, E., Melson, W.G., Thompson, G., 1972. Mineralogy, petrology, and chemical composition of lunar samples 15085, 15256, 15271, 15471, 15475, 15476, 15535, 15555, and 15556. In: 3rd Lunar Sci. Conf. Proc., pp. 785–796.
McCoy, T.J., Lofgren, G.E., 1999. Crystallization of the Zagami shergottite: An experimental study. EPSL 173 (4), 397–411.
Morgan, D.J., Blake, S., 2006. Magmatic residence times of zoned phenocrysts: Introduction and application of the binary element diffusion modelling (BEDM) technique. Contrib. Mineral. Petrol. 151 (1), 58–70.
National Academies of Sciences, Engineering, and Medicine, 2022. Origins, Worlds, and Life: A Decadal Strategy for Planetary Science and Astrobiology 2023–2032. National Academies Press, Washington, DC.
National Research Council (NRC), 2007. The Scientific Context for Exploration of the Moon. National Academies Press, Washington, DC.
Neal, C.R., Donohue, P., Fagan, A.L., O'Sullivan, K., Oshrin, J., Roberts, S., 2015. Distinguishing between basalts produced by endogenic volcanism and impact processes: A non-destructive method using quantitative petrography of lunar basaltic samples. GCA 148, 62–80.
Neal, C.R., Taylor, L.A., 1992. Petrogenesis of mare basalts: A record of lunar volcanism. GCA 56 (6), 2177–2211.
Neave, D.A., Maclennan, J., Hartley, M.E., Edmonds, M., Thordarson, T., 2014. Crystal storage and transfer in basaltic systems: The Skuggafjöll eruption, Iceland. J. Petrol. 55 (12), 2311–2346.
Needham, D.H., Kring, D.A., 2017. Lunar volcanism produced a transient atmosphere around the ancient Moon. EPSL 478, 175–178.
Pankhurst, M.J., Morgan, D.J., Thordarson, T., Loughlin, S.C., 2018. Magmatic crystal records in time, space, and process, causatively linked with volcanic unrest. EPSL 493, 231–241.
Papike, J., Taylor, L., Simon, S., 1991. Lunar minerals. Lunar sourcebook: A user's guide to the Moon, pp. 121–181.
Papike, J.J., Hodges, F.N., Bence, A.E., Cameron, M., Rhodes, J.M., 1976. Mare basalts: Crystal chemistry, mineralogy, and petrology. Rev. Geophys. 14 (4), 475–540.
Rae, A.S., Edmonds, M., Maclennan, J., Morgan, D., Houghton, B., Hartley, M.E., Sides, I., 2016. Time scales of magma transport and mixing at Kīlauea Volcano, Hawai'i. Geology 44 (6), 463–466.
Rhodes, J.M., Hubbard, N.J., 1973. Chemistry, classification, and petrogenesis of Apollo 15 mare basalts. In: 4th Lunar Sci. Conf. Proc., pp. 1127.
Richter, F., Saper, L.M., Villeneuve, J., Chaussidon, M., Watson, E.B., Davis, A.M., Mendybaev, R.A., Simon, S.B., 2021. Reassessing the thermal history of martian meteorite Shergotty and Apollo mare basalt 15555 using kinetic isotope fractionation of zoned minerals. GCA 295, 265–285.
Rumpf, M.E., Fagents, S.A., Crawford, I.A., Joy, K.H., 2013. Numerical modelling of lava-regolith heat transfer on the Moon and implications for the preservation of implanted volatiles. J. Geophys. Res. Planets 118 (3), 382–397.
Ryder, G., Steele, A., 1988. Chemical dispersion among Apollo 15 olivine-normative mare basalts. In: Proc. Lunar Planet. Sci. Conf., 18, pp. 273–282.
Schaber, G.G., Boyce, J.M., Moore, H.J., 1976. The scarcity of mappable flow lobes on the lunar maria: Unique morphology of the Imbrium flows. In: Proc. Lunar Planet. Sci. Conf., 7th, pp. 2783–2800.
Schnare, D.W., Day, J.M., Norman, M.D., Liu, Y., Taylor, L.A., 2008. A laser-ablation ICP-MS study of Apollo 15 low-titanium olivine-normative and quartz-normative mare basalts. GCA 72 (10), 2556–2572.
Shea, T., Lynn, K.J., Garcia, M.O., 2015. Cracking the olivine zoning code: Distinguishing between crystal growth and diffusion. Geology 43 (10), 935–938.
Shearer, C.K., Papike, J.J., 1999. Invited Review. Magmatic evolution of the Moon. Am. Mineral. 84 (10), 1469–1494.
Shearer, C.K., Hess, P.C., Wieczorek, M.A., Pritchard, M.E., Parmentier, E.M., Borg, L.E., Longhi, J., Elkins-Tanton, L.T., Neal, C.R., Antonenko, I., Canup, R.M., 2006. Thermal and magmatic evolution of the Moon. Rev. Mineral. Geochem. 60 (1), 365–518.

Shervais, J.W., Vetter, S.K., Lindstrom, M.M., 1990. Chemical differences between small subsamples of Apollo 15 olivine-normative basalts. In: Proc. Lunar Planet. Sci. Conf., 20, pp. 109–126.
Slater, V.P., Thompson, C.K., Nettles, J., Milam, K., Stockstill, K.R., Cahill, J., Anand, M., Taylor, L.A., 2003. An Evaluation of the Igneous Crystallization Programs–MELTS, MAGPOX, and COMAGMAT Part II: Importance of Magmatic fO2. Lunar and Planetary Institute, p. 1896.
Snape, J.F., Nemchin, A.A., Whitehouse, M.J., Merle, R.E., Hopkinson, T., Anand, M., 2019. The timing of basaltic volcanism at the Apollo landing sites. GCA 266, 29–53.
Snyder, G.A., Borg, L.E., Taylor, L.A., Nyquist, L.E., Halliday, A.N., 1997. Nd–Sr–Hf isotopic and geochronologic studies of Apollo 15 basalts. Lunar Planet. Sci. Conf. 28. Abstract #1505.
Snyder, G.A., Borg, L.E., Taylor, L.A., Nyquist, L.E., Halliday, A.N., 1998. Volcanism in the Hadley-Appenine region of the Moon: geochronology, Nd–Sr isotopic systematics, and depths of melting. Lunar Planet. Sci. Conf. 29. Abstract #1141.
Snyder, G.A., Borg, L.E., Nyquist, L.E., Taylor, L.A., 2000. Chronology and isotopic constraints on lunar evolution. In: Canup, R.M., Righter, K. (Eds.), Origin of the Earth and Moon. University of Arizona Press, Tuscon, pp. 361–395.
Swann, G.A., Bailey, N.G., Batson, R.M., Freeman, V.L., Hait, M.H., Head, J.W., Holt, H. E., Howard, K.A., Irwin, J.B., Larson, K.B., 1972. Preliminary geologic investigation of the Apollo 15 landing site. In Apollo 15 Preliminary Science Report. NASA SP-289 Washington, DC.
Takeda, H., Miyamoto, M., Ishii, T., Lofgren, G.E., 1975. Relative cooling rates of mare basalts at the Apollo 12 and 15 sites as estimated from pyroxene exsolution data. In: 6th Lunar Sci. Conf. Proc, pp. 17–21.
Taylor, L.A., Uhlmann, D.R., Hopper, R.W., Misra, K.C., 1975. Absolute cooling rates of lunar rocks-Theory and application. In: 6th Lunar Sci. Conf. Proc, pp. 181–191.
Taylor, L.A., Onorato, P.I.K., Uhlmann, D.R., 1977. Cooling rate estimations based on kinetic modelling of Fe-Mg diffusion in olivine. In: 8th Lunar Sci. Conf. Proc, pp. 1581–1592.
Thompson, C.K., Slater, V.P., Stockstill, K.R., Anand, M., Nettles, J., Milam, K., Cahill, J., Taylor, L.A., 2003. An Evaluation of the Igneous Crystallization Programs–MELTS, MAGPOX, and COMAGMAT Part I: Does One Size Fit All? Lunar and Planetary Institute, p. 1881.
Thomson, B.J., Grosfils, E.B., Bussey, D.B.J., Spudis, P.D., 2009. A new technique for estimating the thickness of mare basalts in Imbrium Basin. Geophys. Res. Lett. 36 (12), 1–5.
Viccaro, M., Giuffrida, M., Nicotra, E., Cristofolini, R., 2016. Timescales of magma storage and migration recorded by olivine crystals in basalts of the March–April 2010 eruption at Eyjafjallajökull volcano, Iceland. Am. Mineral. 101 (1), 222–230.
Vinet, N., Higgins, M.D., 2010. Magma solidification processes beneath Kilauea volcano, Hawaii: A quantitative textural and geochemical study of the 1969–1974 Mauna Ulu Lavas. J. Petrol. 51 (6), 1297–1332.
Wadhwa, M., 2008. Redox conditions on small bodies, the Moon and Mars. Rev. Mineral. Geochem. 68 (1), 493–510.
Wager, L.R., 1960. The major element variation of the layered series of the Skaergaard intrusion and a re-estimation of the average composition of the hidden layered series and of the successive residual magmas. J. Petrol. 1 (1), 364–398.
Walker, D., Longhi, J., Lasaga, A.C., Stolper, E.M., Grove, T.L., Hays, J.F., 1977. Slowly cooled microgabbros 15555 and 15065. In: 8th Lunar Sci. Conf. Proc, pp. 1521–1547.
Weider, S.Z., Crawford, I.A., Joy, K.H., 2010. Individual lava flow thicknesses in Oceanus Procellarum and Mare Serenitatis determined from Clementine multispectral data. Icarus 209 (2), 323–336.
Wieczorek, M.A., Jolliff, B.L., Khan, A., Pritchard, M.E., Weiss, B.P., Williams, J.G., Hood, L.L., Righter, K., Neal, C.R., Shearer, C.K., McCallum, I.S., 2006. The constitution and structure of the lunar interior. Rev. Mineral. Geochem. 60 (1), 221–364.